The properties of the stellar populations in ULIRGs – I. Sample, data and spectral synthesis modelling

J. Rodríguez Zaurín,[1,2]⋆ C. N. Tadhunter[2] and R. M. González Delgado[3]

[1]*Department of Molecular and Infrared Astronomy, IEM (CSIC), 28006 Madrid, Spain*
[2]*Department of Physics and Astronomy, University of Sheffield, Sheffield S3 7RH*
[3]*Instituto de Astrofisica de Andalucia (CSIC), P.O. Box 3004, 18080 Granada, Spain*

ABSTRACT

We present deep long-slit optical spectra for a sample of 36 ultraluminous infrared galaxies (ULIRGs), taken with the William Herschel Telescope on La Palma with the aim of investigating the star formation histories and testing evolutionary scenarios for such objects. Here we present the sample, the analysis techniques and a general overview of the properties of the stellar populations; a more detailed discussion will be presented in a forthcoming paper. Spectral synthesis modelling has been used in order to estimate the ages of the stellar populations found in the diffuse light sampled by the spectra in both the nuclear and extended regions of the target galaxies. We find that adequate fits can be obtained using combinations of *young stellar populations* (YSPs; $t_{YSP} \leq 2$ Gyr), with ages divided into two groups: *very young stellar populations* (VYSPs; $t_{VYSP} \leq 100$ Myr) and *intermediate-young stellar populations* (IYSPs; $0.1 < t_{IYSP} \leq 2$ Gyr). Our results show that YSPs are present at *all* locations of the galaxies covered by our slit positions, with the exception of the northern nuclear region of the ULIRG IRAS 23327+2913. Furthermore, VYSPs are present in at least 85 per cent of the 133 extraction apertures used for this study, being more significant in the nuclear regions of the galaxies. *Old stellar populations* (OSPs; $t_{OSP} > 2$ Gyr) do not make a major contribution to the optical light in the majority of the apertures extracted. In fact they are essential for fitting the spectra in only 5 per cent (seven) of the extracted apertures. The estimated total masses for the YSPs (VYSPs + IYSPs) are in the range $0.18 \times 10^{10} \leq M_{YSP} \leq 50 \times 10^{10}$ M$_\odot$. We have also estimated the bolometric luminosities associated with the stellar populations detected at optical wavelengths, finding that they fall in the range $0.07 \times 10^{12} < L_{bol} < 2.2 \times 10^{12}$ L$_\odot$. In addition, we find that reddening is significant at all locations in the galaxies. This result emphasizes the importance of accounting for reddening effects when modelling the stellar populations of star-forming galaxies.

Key words: galaxies: evolution – galaxies: starburst.

1 INTRODUCTION

The launch of the *Infrared Astronomical Satellite (IRAS)* in 1983 triggered a development of infrared (IR) astronomy that is still ongoing. Although the majority of the sources discovered by *IRAS* were modest IR emitters, some objects had mid- to far-infrared (MFIR) luminosities comparable to the bolometric luminosities of optically selected quasi-stellar objects (QSOs; Houck et al. 1984, 1985; Soifer et al. 1984a,b, 1987). Such galaxies are classified as luminous ($L_{ir} > 10^{11}$ L$_\odot$) or ultraluminous ($L_{ir} > 10^{12}$ L$_\odot$) infrared galaxies (LIRGs/ULIRGs) depending on their MFIR luminosities.

The prodigious IR emission of ULIRGs is generally attributed to the optical/ultraviolet (UV) light of luminous central sources reprocessed by dust. Several IR spectroscopic studies have provided evidence that the power source of ULIRGs has a composite nature, with a mixture of active galactic nucleus (AGN) and starburst activity (Genzel et al. 1998; Lutz, Veilleux & Genzel 1999; Armus et al. 2007; Farrah et al. 2007; Imanishi et al. 2007). Similar conclusions are reached in the relatively few studies carried out at UV/optical (Veilleux et al. 1995; Veilleux, Kim & Sanders 1999a; Farrah et al. 2003) and X-ray (Franceschini et al. 2001, 2003) wavelengths. Therefore, these objects provide us with an excellent opportunity to study the links between AGN and starburst phenomena. In addition, ULIRGs are almost invariably associated with galaxy mergers and interactions (e.g. Kim, Veilleux & Sanders

⋆E-mail: jrz@damir.iem.csic.es

Table 1. The CS of 26 ULIRGs with redshifts $z < 0.13$ and declinations $\delta > -23°$. Column (1): object designation in the *IRAS* Bright Galaxy survey (Soifer et al. 1986, 1987). Column (2): optical redshifts from Kim & Sanders (1998). Columns (3) and (4): right ascension (hours, minutes and seconds) and declination (degrees, arcminutes and arcseconds) of the *IRAS* source position as listed in the Faint Source Data base (FSDB). Column (5): IR luminosity from Kim & Sanders (1998). Column (6): f_{25}/f_{60} MFIR colour ratio, where f_{25} and f_{60} represent the *IRAS* flux densities (non-colour corrected) in units of Jy at 25 and 60 μm, respectively. Columns (5) and (6): both from Kim & Sanders (1998). Column (7): nuclear structure (from Kim et al. 2002). Column (8): nuclear separation (NS) from Veilleux et al. (2002). Column (9): interaction class: class I: first approach; class II: first contact; class III: pre-merger; class IV: merger; class V: old merger; Tpl: triple; Iso: isolated (see Veilleux et al. 2002, for details). Column (10): optical nuclear spectral type (from Veilleux et al. 1995; Kim & Sanders 1998; Veilleux et al. 1999a): H: H II; L: LINER; S1: Seyfert 1; S2: Seyfert 2.

Object name IRAS	z	RA (J2000.0)	Dec. (J2000.0)	log L_{ir} (L$_\odot$)	f_{25}/f_{60}	Nuclear structure	NS (kpc)	IC	ST
(1)	(2)	(3)	(4)	(5)	(6)	(7)	(8)	(9)	(10)
00091−0738	0.118	00 11 43.4	−07 22 06	12.23	0.08	Double	2.2	IIIb	H
00188−0856	0.128	00 21 26.0	−08 39 29	12.37	0.14	Single	–	V	L
01004−2237	0.129	01 02 51.2	−22 21 51	12.28	0.28	Single	–	V	H
12072−0444^a	0.129	12 09 45.4	−05 01 14	12.39	0.21	Double	2.8	IVb	S2
12112+0305	0.073	12 13 47.3	02 48 34	12.32	0.06	Double	4.0	IIIb	L
12540+5708	0.042	12 56 15.0	56 52 17	12.54	0.27	Single	–	IVb	S1
13428+5608^a	0.037	13 44 41.8	55 53 14	12.14	0.10	Double	0.7	IVb	S2
13451+1232	0.122	13 47 33.3	12 17 24	12.32	0.35	Double	4.2	IIIb	S2
13539+2920	0.108	13 56 10.9	29 05 29	12.04	0.06	Double	7.4	IIIb	H
14060+2919	0.117	14 .08 17.5	29 04 57	12.07	0.08	Single	–	IVa	H
14348−1447	0.083	14 37 37.3	−15 00 20	12.32	0.07	Double	5.1	IIIb	L
14394+5332^b	0.105	14 41 04.3	53 20 08	12.08	0.17	Multiple	54.0	Tpl	S2
15130−1958	0.109	15 15 55.6	−20 09 18	12.09	0.20	Single	–	IVb	S2
15206+3342	0.125	15 22 38.0	33 31 36	12.22	0.20	Single	–	IVb	H
15327+2340	0.018	15 34 57.1	23 30 10	12.21	0.07	Double	0.4	IIIb	L
15462−0450	0.100	15 48 56.6	−04 59 36	12.21	0.15	Single	–	IVb	S1
16474+3430	0.111	16 49 14.7	34 25 13	12.15	0.09	Double	6.9	IIIb	H
16487+5447	0.104	16 49 47.8	54 42 34	12.16	0.07	Double	5.7	IIIb	L
17028+5817	0.106	17 03 41.8	58 13 48	12.14	0.04	Double	24.6	IIIa	L
20414−1651	0.086	20 44 17.4	−16 40 14	12.18	0.08	Single	–	IVb	H
21208−0519	0.130	21 23 28.7	−05 06 59	12.05	0.13	Double	14.9	IIIa	H
21219−1757	0.112	21 24 42.5	−17 44 40	12.10	0.42	Single	–	IVa	S1
22491−1808	0.076	22 51 49.0	−17 52 27	12.13	0.10	Double	2.4	IIIb	H
23233+2817	0.114	23 25 48.7	28 34 19	12.04	0.22	Single	–	Iso.	S2
23234+0946	0.128	23 25 56.0	10 02 52	12.09	0.05	Double	7.8	IIIb	L
23327+2913	0.107	23 35 12.5	29 30 05	12.10	0.10	Double	24.0	IIIa	L

^{a}Kim et al. (2002) classified these objects as single nucleus systems. However, a double nucleus structure is revealed in the studies of Dasyra et al. (2006a) and Scoville et al. (2000) for IRAS 12072−0444 and IRAS 13428+5608, respectively. These objects will be classified as double nucleus systems for the work presented here.
^{b}This source is a multiple (>2 nucleus) system. The two main components are separated 54 kpc, but the eastern component itself comprises two close nuclei.

2002; Veilleux, Kim & Sanders 2002). Thus, they also represent ideal objects to test models of galaxy evolution via major galaxy mergers (e.g. Barnes & Hernquist 1996; Mihos & Hernquist 1996; Springel et al. 2005).

Stellar population studies have the potential to provide key information about the histories of the merger events associated with ULIRGs. To date, two complementary approaches have been used to investigate the stellar populations in such objects: one based on photometric analysis of images of the galaxies taken at different wavelengths, focused mainly on studying the young stellar populations (YSPs) associated with the bright knots (Surace et al. 1998; Surace & Sanders 1999, 2000; Surace, Sanders & Evans 2000; Wilson et al. 2006); the other comprising spectroscopic analysis of UV/optical spectra (Canalizo & Stockton 2000a,b, 2001; Farrah et al. 2005; Rodríguez Zaurín et al. 2007, hereafter RZ07; Rodríguez Zaurín, Tadhunter & González Delgado 2008, hereafter RZ08). Overall, there have been relatively few studies of the stel-

lar populations in ULIRGs. The existing studies mentioned above either concern relatively small samples of ULIRGs, or concentrate on high surface brightness regions which may give a misleading impression of the stellar populations of the systems as a whole.

To remedy this situation we have obtained deep, wide spectral coverage, intermediate-resolution long-slit spectroscopic observations for a sample of 36 ULIRGs with redshifts $z < 0.18$ using the ISIS (Intermediate dispersion Spectrograph and Imaging System) spectrograph on the William Herschel Telescope (WHT). With the aim of studying in detail the properties of the stellar populations in the ULIRGs in our sample, and thereby testing evolutionary scenarios, we model the spectra extracted from a series of apertures using a large number of different combinations of stellar populations synthesis model templates (Bruzual & Charlot 2003). In this paper we present the sample and the spectral synthesis modelling results, while a more detailed analysis of the results is presented in the forthcoming paper (Rodríguez Zaurín et al., in preparation). Detailed

Table 2. Same as Table 1, but for the 10 additional objects included in the ES discussed in this paper.

| Object name IRAS	z	RA (J2000.0)	Dec. (J2000.0)	log L_{ir} ($L_\odot$)	f_{25}/f_{60}	Nuclear structure	NS (kpc)	IC	ST
(1)	(2)	(3)	(4)	(5)	(6)	(7)	(8)	(9)	(10)
08572+3915	0.058	09 00 25.0	39 03 56	12.15	0.22	Double	6.0	IIIb	L
10190+1322	0.077	10 21 41.9	13 07 01	12.04	0.11	Double	5.9	IIIb	H
10494+4424	0.092	10 52 22.2	44 08 59	12.17	0.04	Single	–	IVb	L
13305−1739	0.148	13 33 15.2	−17 55 01	12.25	0.33	Single	–	V	S2
14252−1550	0.149	14 28 01.4	−16 03 43	12.19	0.20	Double	8.8	IIIb	L
16156+0146	0.132	16 18 08.2	01 39 21	12.08	0.24	Double	8.0	IIIb	S2
17044+6720	0.135	17 04 28.5	67 16 34	12.17	0.28	Single	–	IVb	L
17179+5444	0.147	17 18 55.1	54 41 50	12.24	0.14	Single	–	IVb	S2
23060+0505	0.173	23 08 34.2	05 21 29	12.48	0.37	Single	–	IVb	S2
23389+0303	0.145	23 41 31.1	03 17 31	12.13	0.28	Double	5.2	IIIb	S2
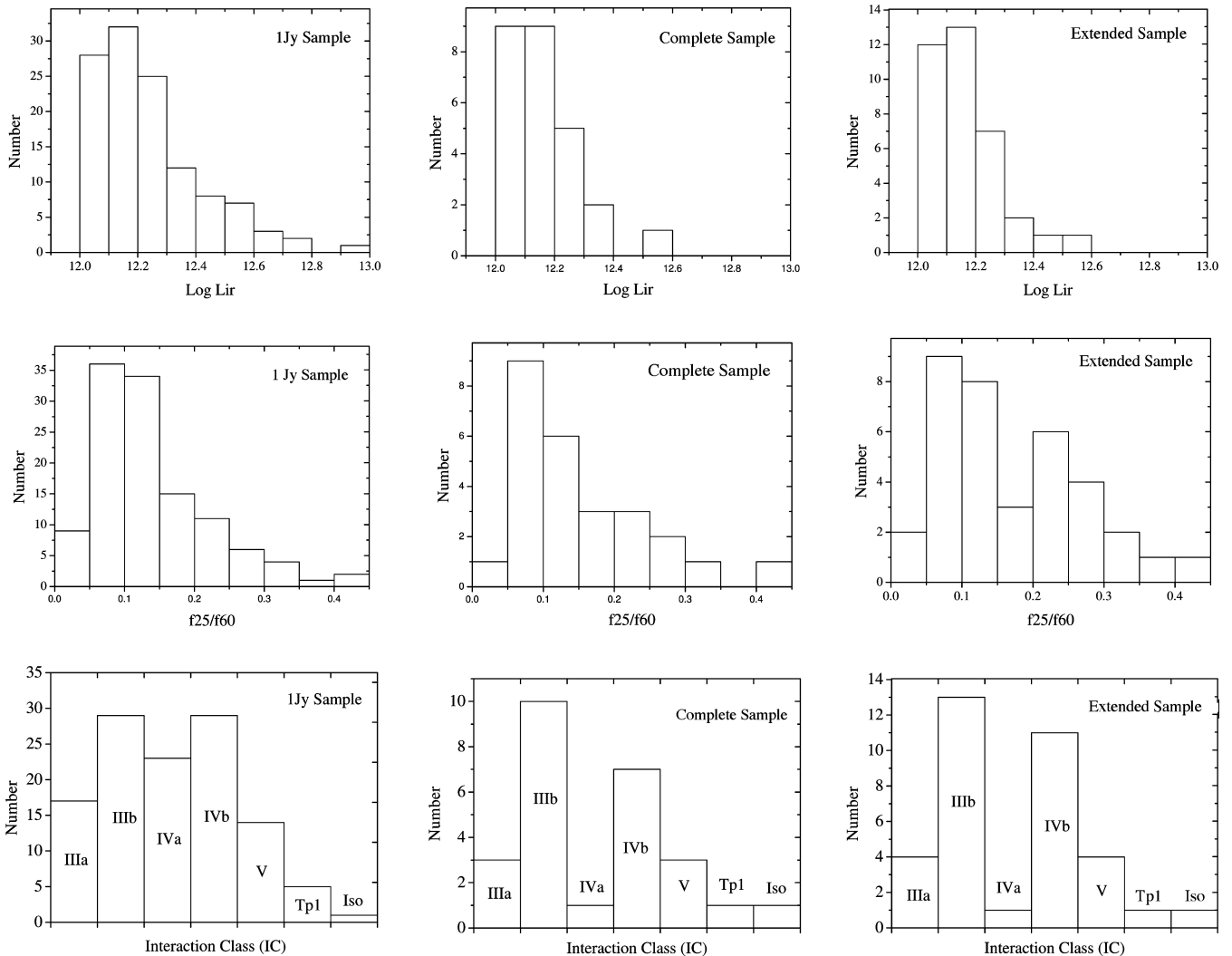
Figure 1. Upper panel: histograms showing the IR luminosity distributions for the full 1-Jy sample of Kim & Sanders (1998), the CS and the ES. The figure shows that both the CS and the ES are representative of the 1-Jy sample in terms of IR luminosities. Middle panel: same as the upper panel, but for the f_{25}/f_{60} μm ratio, used to classify the ULIRGs as cold ($f_{25}/f_{60} < 0.2$) or warm ($f_{25}/f_{60} \geq 0.2$) objects. The figure shows that the CS is representative of the 1-Jy sample in terms of the f_{25}/f_{60} ratio distribution. On the other hand, as expected, the ES is biased towards warm objects. Lower panel: same as the upper panel, but for the interaction class distribution, using the morphological classification scheme described in Veilleux et al. (2002). The figure shows that the CS and the ES both have similar distributions of objects in interaction class to the 1-Jy sample, with the exception of the IVa class (see the text for an explanation).

Table 3. Log of the spectroscopic observations. In the case of Arp 220 (IRAS 15327+2340), a slit in PA 75 was also used with 10 arcsec offset to the north, with respect to the one referred as PA75 in the table: this is labelled as PA75*. The seeing was estimated from DIMM seeing monitor measurements.

Object name IRAS (1)	PA (○) (2)	Arm (3)	Exposure (s) (4)	Airmass (5)	Seeing FWHM (arcsec) (6)
00091−0738	0	B	2700	1.24	1.2
		R	2700	1.24	1.2
00188−0856	332	B	2100	1.33–1.37	1.3
		R	2100	1.33–1.37	1.3
01004−2237	352	B	2100	1.60	2.8
		R	2100	1.60	2.8
08572+3915	265	B	3600	1.14–1.32	1.3
		R	3600	1.14–1.32	1.3
10190+1322	64	B	3600	1.04	1.2
		R	3600	1.04	1.2
10494+4424	167	B	3600	1.03–1.07	1.2
		R	3600	1.03–1.07	1.2
12072−0444	45	B	2700	1.30–1.42	1.1
		R	2700	1.30–1.42	1.1
12112−0305	15	B	2700	1.11	1.2
		R	2700	1.11	1.2
12540+5708	180	B	2700	1.13	0.7–1.6
		R	2700	1.13	0.7–1.6
13305−1739	342	B	2700	1.53–1.62	1.7
		R	2700	1.53–1.62	1.7
13428+5608	180	B	2700	1.12	1.7
		R	2700	1.12	1.7
13451+1232	160	B	3600	1.05	1.3
		R	3600	1.05	1.3
	230	B	3600	1.1	1.7
		R	3600	1.1	1.7
13539+2920	285	B	2700	1.01	1.1–1.6
		R	2700	1.01	1.1–1.6
14060+2919	83	B	2700	1.06–1.11	0.9–1.3
		R	2700	1.06–1.11	0.9–1.3
14252−1550	40	B	2700	1.63–1.82	0.8
		R	2700	1.63–1.82	0.8
14348−1447	35	B	2700	1.61–1.80	1.4–2.1
		R	2700	1.61–1.80	1.4–2.1
14394+5332	92	B	3600	1.47–1.70	1.6
		R	3600	1.47–1.70	1.6
15130−1958	358	B	2700	1.53	0.8–1.1
		R	2700	1.53	0.8–1.1
15206+3342	90	B	2700	1.23–1.28	0.9–1.8
		R	2700	1.23–1.28	0.9–1.8
15327+2340	160	B	2700	1.03–1.07	1.3–2.0
		R	2700	1.03–1.07	1.3–2.0
	75	B	2700	1.14–1.19	0.6
		R	2700	1.14–1.19	0.6
	75*	B	3600	1.27–1.46	0.7
		R	3600	1.27–1.46	0.7
15462−0450	10	B	2700	1.2	1.6
		R	2700	1.2	1.6
16156+0146	313	B	2700	1.16–1.21	1.2–1.7
		R	2700	1.16–1.21	1.2–1.7
16474+3430	166	B	2700	1.01	1.0
		R	2700	1.01	1.0
16487+5447NE	110	B	2700	1.12	1.2
		R	2700	1.12	1.2
16487+5447NW	165	B	2700	1.26–1.32	1.1
		R	2700	1.26–1.32	1.1
17028+5817NE	130	B	2700	1.23–1.28	1.2
		R	2700	1.23–1.28	1.2

Table 3 – *continued*

Object name IRAS	PA (∘)	Arm	Exposure (s)	Airmass	Seeing FWHM (arcsec)
(1)	(2)	(3)	(4)	(5)	(6)
17028+5817NW	110	B	2700	1.31–1.39	0.9
		R	2700	1.31–1.39	0.9
17044+6720	160	B	2700	1.20–1.29	1.4–1.9
		R	2700	1.20–1.29	1.4–1.9
17179+5444	122	B	2700	1.22–1.28	0.9
		R	2700	1.22–1.28	0.9
20414−1651	5	B	2700	1.42	1.4–1.7
		R	2700	1.42	1.4–1.7
21208−0519	15	B	2700	1.20	1.2
		R	2700	1.20	1.2
21219−1757	333	B	3600	1.54–1.67	1.5
		R	3600	1.54–1.67	1.5
22491−1808	338	B	3600	1.54–1.58	1.0–1.5
		R	3600	1.54–1.58	1.0–1.5
23060+0505	338	B	3600	1.09–1.13	0.7
		R	3600	1.09–1.13	0.7
23233+2817	168	B	2100	1.00	1.2
		R	2100	1.00	1.2
23234+0946	115	B	2700	1.06	1.1
		R	2700	1.06	1.1
23327+2913	175	B	2700	1.00	1.7
		R	2700	1.00	1.7
23389+0300	24	B	3600	1.12	0.7
		R	3600	1.12	0.7

analyses of two of the objects in the sample, IRAS 13451+1232 (PKS 1345+12) and IRAS 15327+2340 (Arp 220), were presented in RZ07 and RZ08, respectively.

Throughout this paper, we assume a cosmology with $H_0 = 71 \, \mathrm{km \, s^{-1} \, Mpc^{-1}}$, $\Omega_0 = 0.27$, $\Omega_\Lambda = 0.73$. All the values presented in this paper have been adapted to this cosmology.

2 OBSERVATIONS AND DATA REDUCTION

2.1 The sample

In the first place, we observed a complete right ascension (RA) and declination (Dec.) limited subsample of the Kim & Sanders (1998) 1-Jy sample of ULIRGs,[1] with RAs in the range $12 < \mathrm{RA} < 1:30$ h, declinations $\delta > -23°$ and redshifts $z < 0.13$. The redshift limit was chosen to ensure that the objects are sufficiently bright for spectroscopic study, and also to keep the size of the sample tractable for deep observations on 4-m class telescopes. Throughout the paper, we will refer to this sample of 26 objects as the complete sample (CS). Table 1 summarizes some of the properties of the ULIRGs in the CS.

As shown in the table, only eight ULIRGs with warm MFIR colours $(f_{25}/f_{60} > 0.2)$[2] are included in the CS. However, one of the aims of the project was to study the presence of an evolutionary link between cool and warm ULIRGs. Therefore, we

extended the sample to include six higher redshift objects classified as warm ULIRGs: IRAS 13305−1739, IRAS 14252−1739, IRAS 16156+0146, IRAS 17044+6720, IRAS 23060+0505 and IRAS 23389+0303. In addition, since we also aim to test the evolutionary scenario in which ULIRGs evolve into QSOs or a radio galaxies (e.g. Surace et al. 1998; Surace & Sanders 1999; Canalizo & Stockton 2001; Tadhunter et al. 2005), we decided to include IRAS 17179+5444, which is classified as a cool ULIRG with a type 2 Seyfert (Sy2)-like optical spectrum. Finally, three ULIRGs were included in the sample (IRAS 08572+3915, IRAS 10190+1322 and IRAS 10494+4424) which have redshifts $z < 0.13$, but fall outside the RA range of the CS. One of them, IRAS 08572+3915, is classified as a warm ULIRG. Thus, the total sample discussed in this paper comprises 36 objects: 21 cool ULIRGs and 15 warm ULIRGs. We will refer to this sample as the extended sample (ES). With an upper limiting redshift of $z < 0.18$, the ES includes all the warm ULIRGs within the RA and Dec. range of the CS with redshifts $z < 0.15$. Table 2 summarizes some of the properties of the 10 ULIRGs which, together with the CS, comprise the ES. Optical and near-IR images for all the objects in the ES are presented in Kim et al. (2002).

Fig. 1 presents histograms comparing the full 1-Jy sample, the CS and the ES in terms of IR-luminosity, f_{25}/f_{60} flux ratio and morphological type distributions, respectively. The upper panel shows that both the CS and the ES are representative of the 1-Jy sample in terms of IR-luminosities, while the middle panel of the figure shows that, as expected, the ES is biased towards objects classified as warm ULIRGs $(f_{25}/f_{60} > 0.2)$. Using the morphological classification scheme described in Veilleux et al. (2002), the lower panel in Fig. 1 shows the distribution of the different morphological types of the objects comprising each sample. To summarize (see Veilleux et al. 2002, for further details), the different classes are class I (first approach), class II (first contact), class III (pre-merger), class IV

---

[1] This is in itself a complete flux-limited sample of 118 ULIRGs identified from the *IRAS* Faint Source Catalogue (FSC) and selected to have a 60 µm flux densities greater than 1 Jy in a region of the sky with $\delta > -40°$ and $|b| > 30°$.

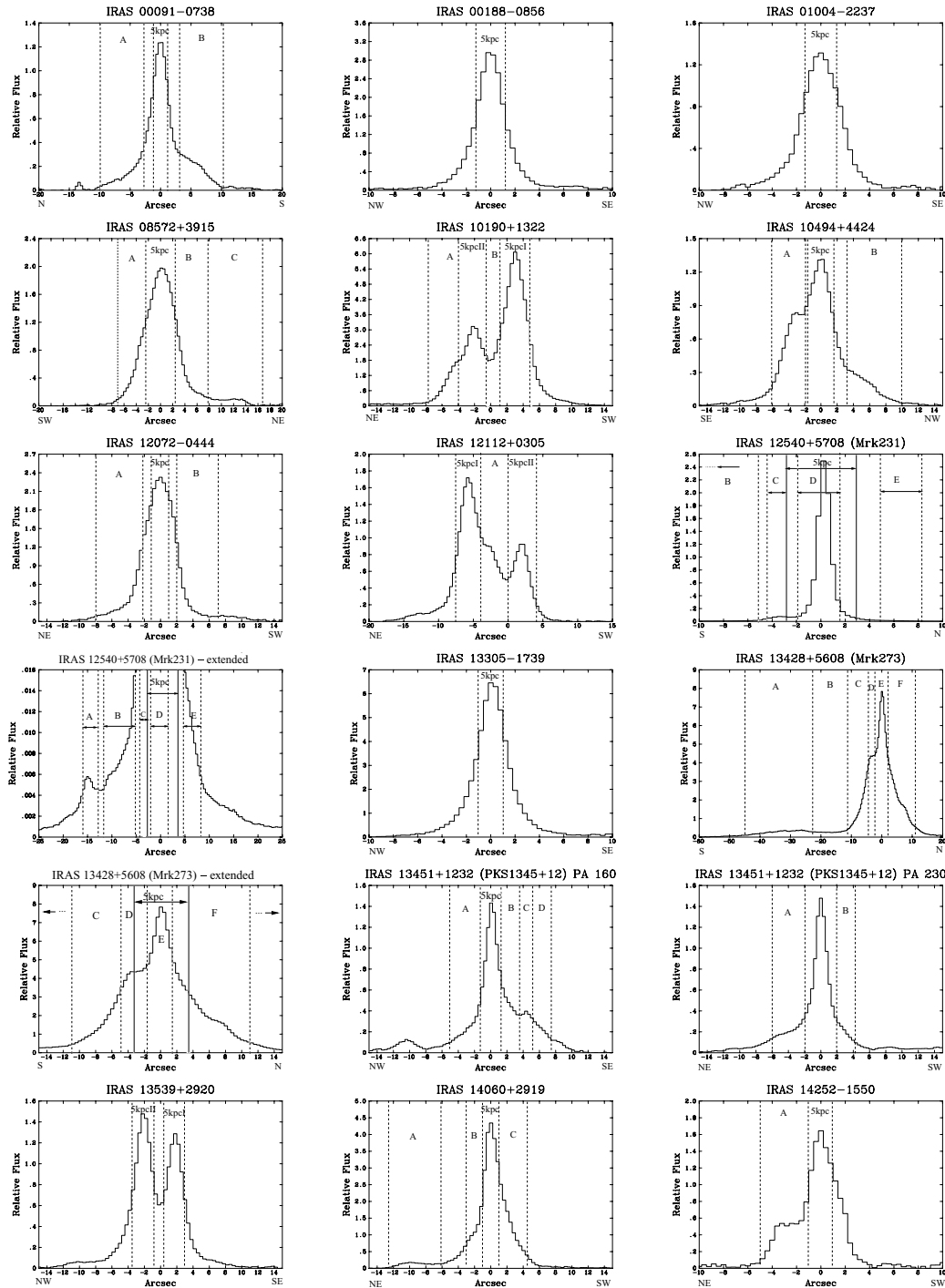[2] The quantities f_{25} and f_{60} represent the *IRAS* flux densities in Janskys at 25 and 60 µm.

Figure 2. Spatial profiles of the 2D spectra for the wavelength range 4400–4600 Å showing the positions of the extraction apertures. The symbols N, S, E and W at the positive and negative ends of the *x*-axis represent the directions of the slit on the sky. For example, in the case of IRAS 00091−0738, positive *x* corresponds to south, negative *x* corresponds to north.

(merger), class V (old merger), Tpl (triple) and Iso (isolated). As is clear in the figure, both the CS and the ES samples account for most of the morphological types of objects found in the full 1-Jy sample, with the exception of those classified as IVa.[3] This is due to

___

[3] In the Veilleux et al. (2002) morphological classification, objects classified as IVa are those with prominent tidal features and diffuse extended central regions, but only one nucleus.

the fact that all but four of the IVa sources in the 1-Jy sample are at redshifts $z > 0.13$ (one of these four sources, IRAS 14060+2919, is included in the CS), and the objects in the CS are selected at low ($z < 0.13$) redshifts. In addition, among the 23 objects classified as IVa in the 1-Jy sample, only one is classified as a warm ULIRG, and therefore, these objects were not selected, a priori, to be observed and included in the ES. To summarize, the CS and the ES samples are representative of ULIRGs in the local Universe, although the ES contains a higher proportion of warm objects.
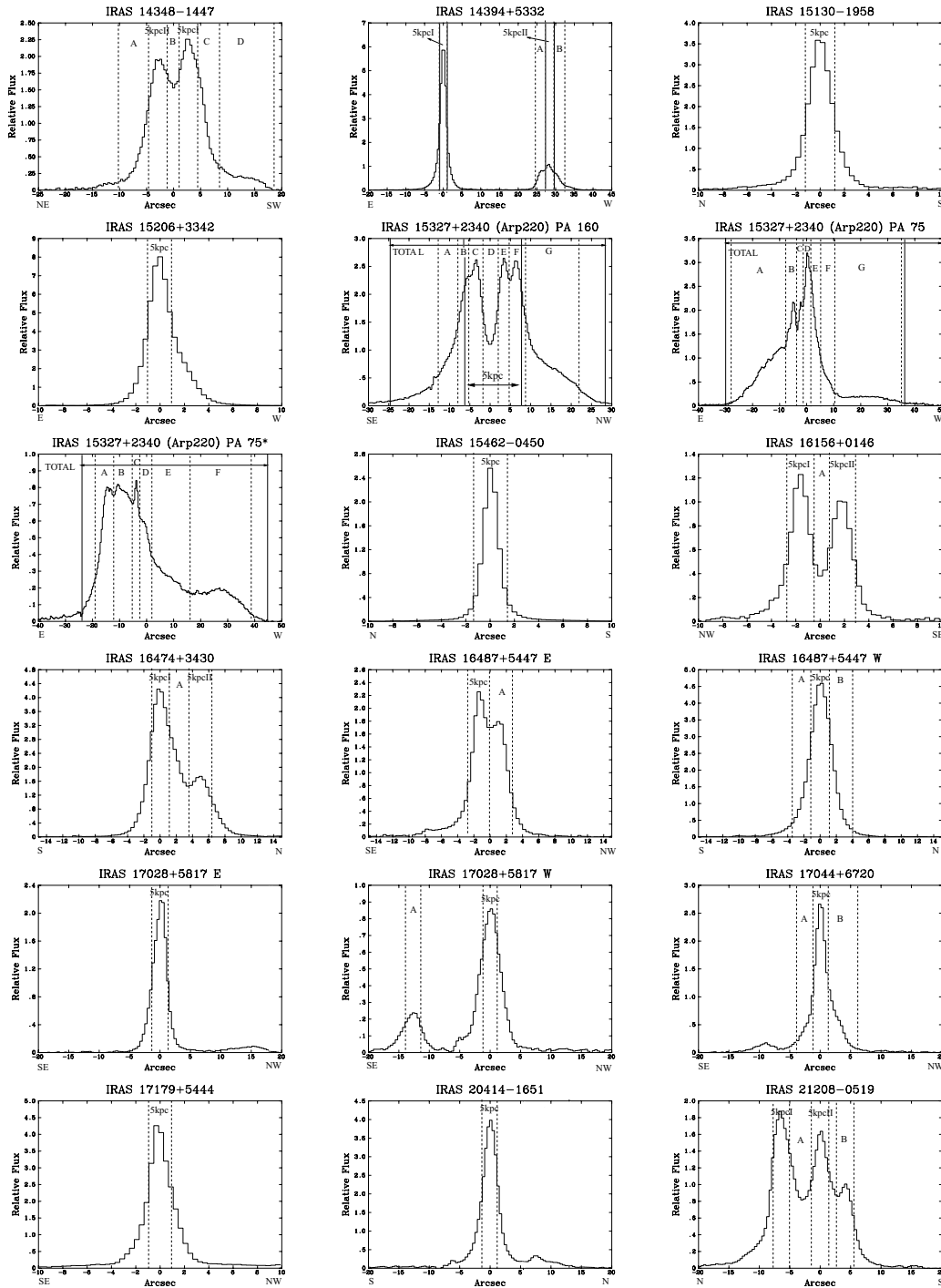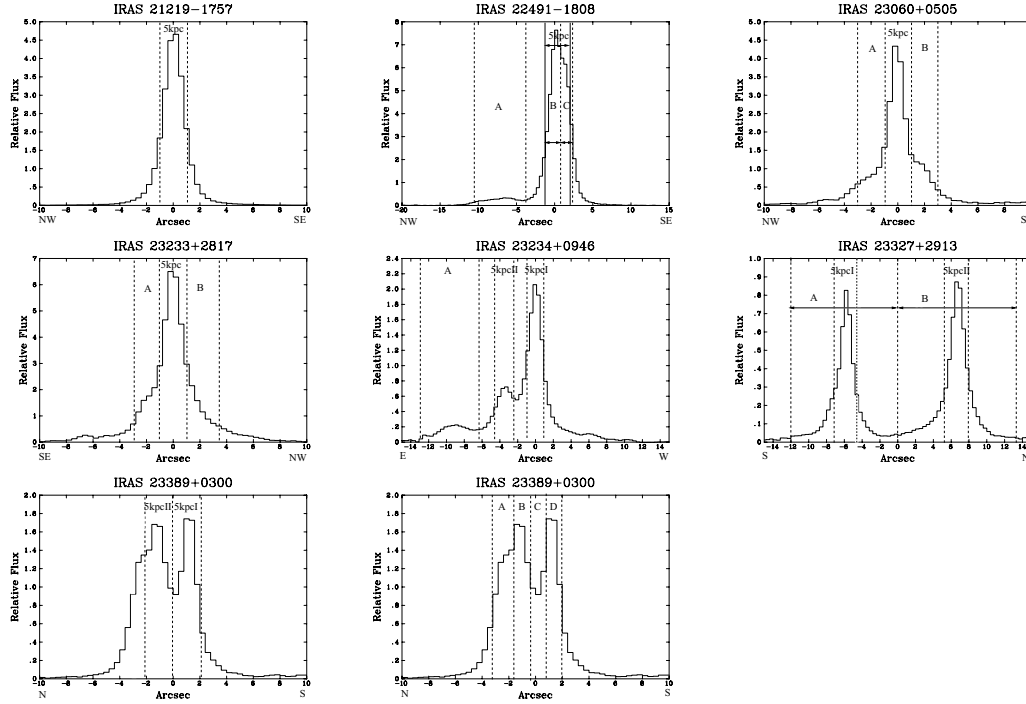
Figure 2 – *continued*

2.2 Optical spectroscopy

Long-slit spectra of all the objects in the ES were taken in 2005 July, 2005 December and 2006 May/July, with the ISIS dual-beam spectrograph on the 4.2-m WHT, on La Palma, Spain. With the exception of IRAS 22491−1808, described below, we used the R300B grating with the EEV12 CCD, and the R316R grating with the MARCONI2 CCD on the blue arm and the red arm respectively, along with a dichroic cutting at ∼5300 Å. A 2 × 2 binning mode was used during the observations, leading to a final spatial scale of 0.4 arcsec pixel^{-1}

for both arms, and a dispersion of 1.72 Å pixel^{-1} in the blue and 1.65 Å pixel^{-1} in the red arm. The observed useful wavelength range is ∼3300–7800 Å. A slit of width 1.5 arcsec was used for all the objects in the ES. In the case of IRAS 22491−1808, the settings in the blue arm were the same as described above. However, on the red arm, the R600R grating with the MARCONI2 CCD was used, with 2 × 2 binning mode. The final spatial scale was 0.4 arcsec pixel^{-1} and the dispersion was 0.89 Å pixel^{-1}. The observed useful wavelength range is ∼3300–7100 Å. Details of the observations for all the objects included in the ES are presented in Table 3.

Figure 2 – *continued*

The position angles (PA) of the slit were carefully selected to cover the main features of the objects (nuclei, tidal tail, bridges, knots). In order to minimize the effects of differential atmospheric refraction, the objects were observed either along parallactic angle or at small airmass (AM < 1.1). For those objects with a double nucleus structure, the slits covered both nuclei, with the exceptions of IRAS 08572+3915 and PKS 1345+12, for which it was not possible to observe the object at the parallactic angle and we did not have sufficient time to observe both nuclei during the night of the observations. In the cases of the double nucleus objects IRAS 16487+5447 and IRAS 17028+5817, because of the parallactic angle constraints, the two nuclei in each system were observed with separate slit PAs.

The data were reduced (bias subtracted, flat-field corrected, cleaned of cosmic rays, wavelength calibrated and flux calibrated) and straightened before extraction of the individual spectra using the standard packages in IRAF and the STARLINK packages FIGARO and DIPSO. The wavelength calibration accuracy, measured as the mean shift between the measured and published (Osterbrock et al. 1996) wavelength of night-sky emission lines, is ~0.35 Å for the blue spectra and ~0.25 Å for the red spectra. No significant variations of these values were found for the observations of the objects comprising the sample used in this paper. The spectral resolutions, calculated using the widths of the night-sky emission lines [full width at half-maximum (FWHM)], are in the ranges of 3.4–6.03 and 4.44–5.84 Å for the blue and red arms, respectively.

Accurate relative flux calibration is vital for the purpose of this project, and therefore several (four–six) photometric standard stars were observed during each night of the observations. The relative flux calibration accuracy is estimated to be ±5 per cent over the entire useful spectral range (~3300–7800 Å). This is confirmed by the excellent match between the fluxes in the overlapping region of the blue and red arm spectra.

3 ANALYSIS

3.1 Aperture extraction

The relatively low redshifts of the objects in the ES, the wide spectral coverage, intermediate spectral resolution, excellent flux calibration and high signal-to-noise ratio (S/N) of the spectra, make it possible to perform detailed studies of their stellar populations. The extraction apertures were selected from spatial cuts of the two-dimensional (2D) frames in the line-free continuum wavelength range 4400–4600 Å, based on the visible extended structures and the requirement that the apertures are large enough to have a sufficiently high S/N for further analysis. In order to compare the stellar populations between the objects in our sample, apertures with a metrical scale of 5 kpc centred on the main nuclei were extracted for all the objects in the ES, including separate extractions for multiple nuclei in individual sources. As mentioned before, a detailed analysis of the particular cases of IRAS 1341+1232 (PKS 1345+12) and IRAS 15327+2740 (Arp 220) can be found in RZ07 and RZ08, respectively. In the case of PKS 1345+12 the aperture labelled as 'NUC AP' in the RZ07 paper has a metric scale of 5.2 kpc and, hereafter, we will refer to this as the 5-kpc aperture for this galaxy. In the case of Arp 220, the closest object in the sample ($z = 0.018$, resulting in a scale of 0.363 kpc arcsec^{-1} and a distance of 77.6 Mpc), a 5-kpc aperture covers a large region of the slit and, therefore, was not selected a priori when performing the study presented in RZ08. In order to compare Arp 220 with the other ULIRGs included in the sample used for the work presented here, we used the slit with PA 160 and extracted a 5-kpc aperture, as shown in Fig. 2, sampling the central region of the galaxy (see fig. 1 in RZ08). A second set of apertures was then selected to sample the spatial features of those objects in the ES showing tails, bridges and other diffuse structures. A total of 133 apertures was extracted for the ULIRGs in the ES.
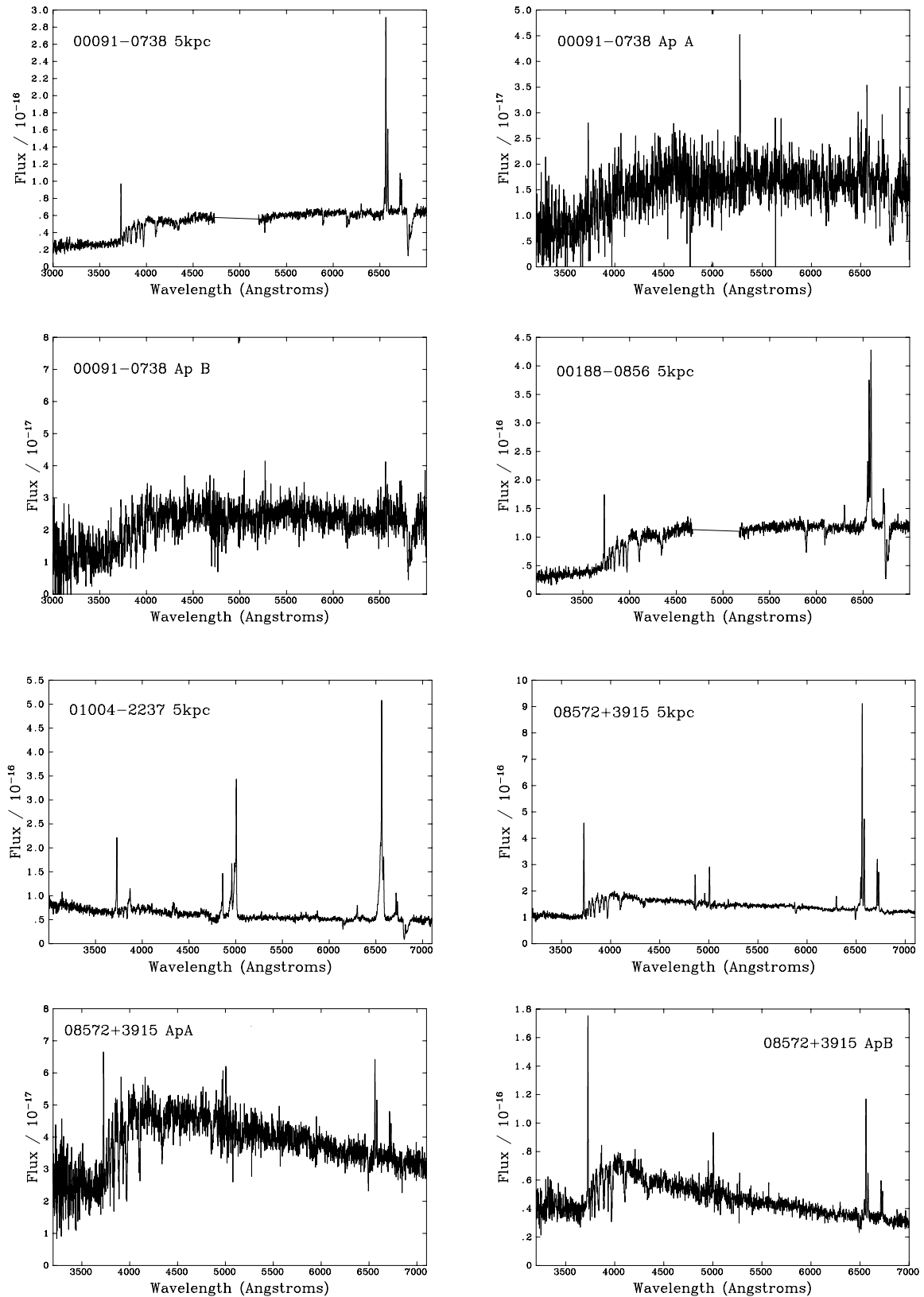
Figure 3. The extracted 1D spectra for all the ULIRGs and apertures in the ES. When the dichroic effects are important, it is not possible to show an adequate plot of the entire wavelength range, and the dichroic region is removed from the plots. The fluxes are presented in wavelength units.
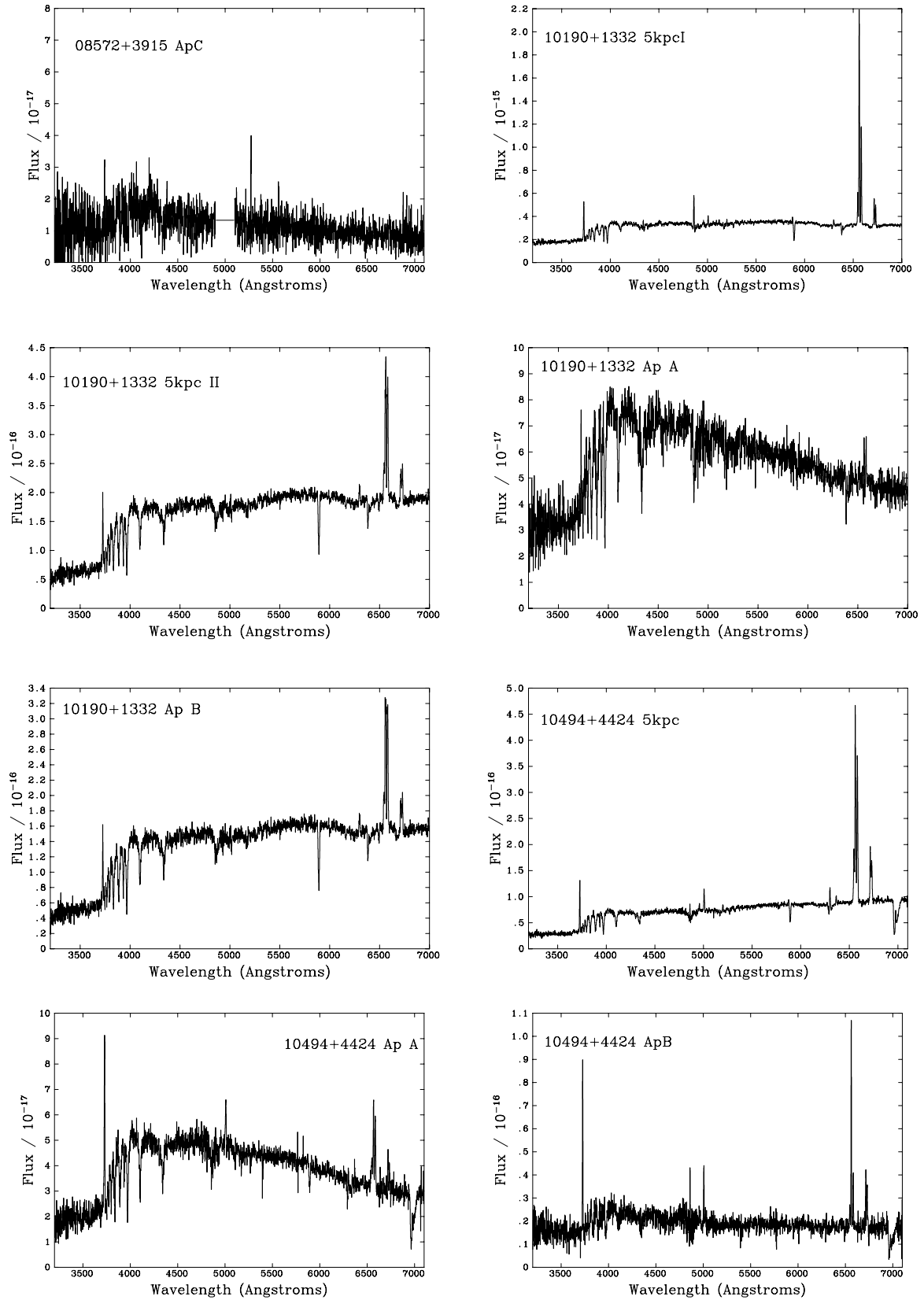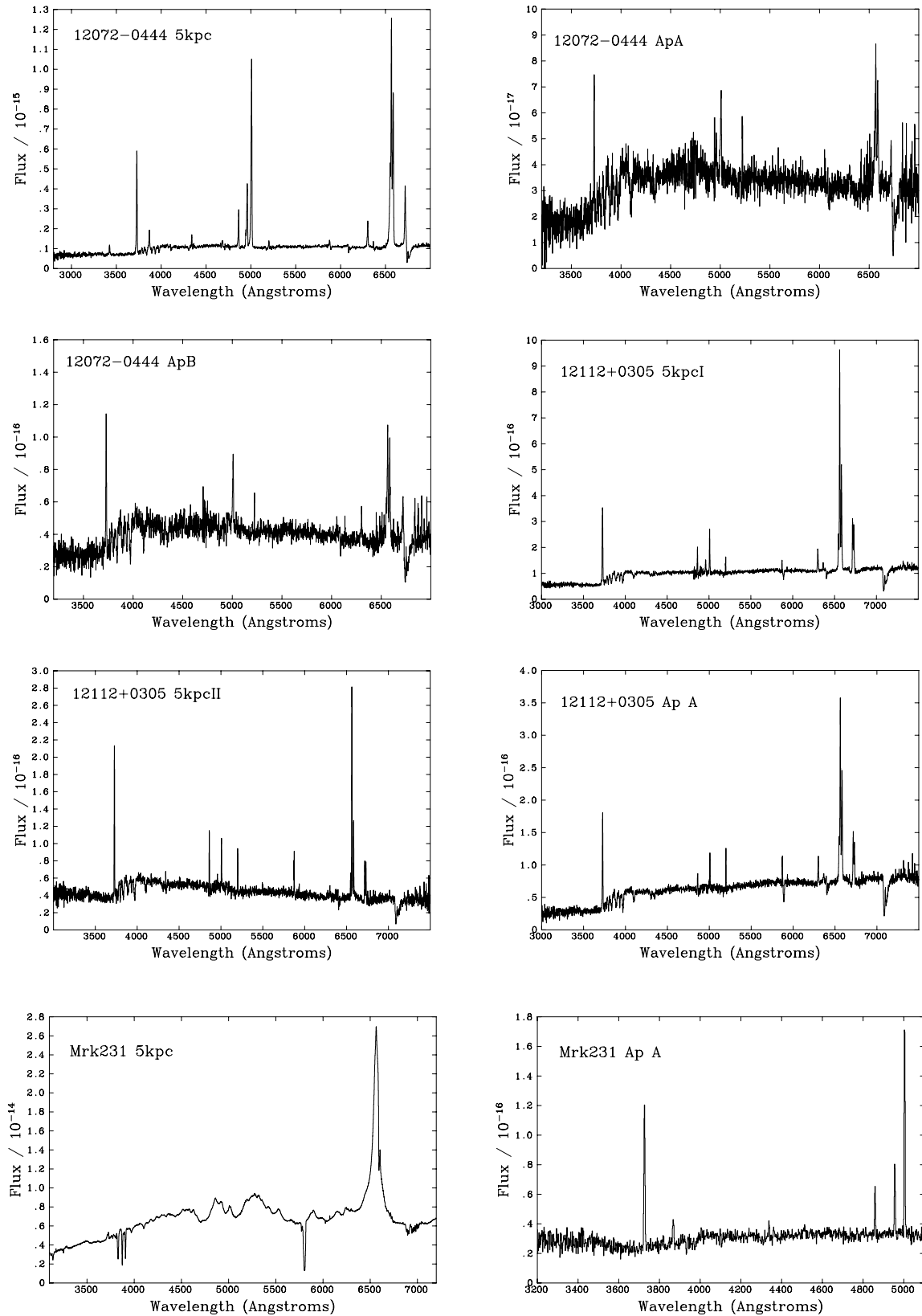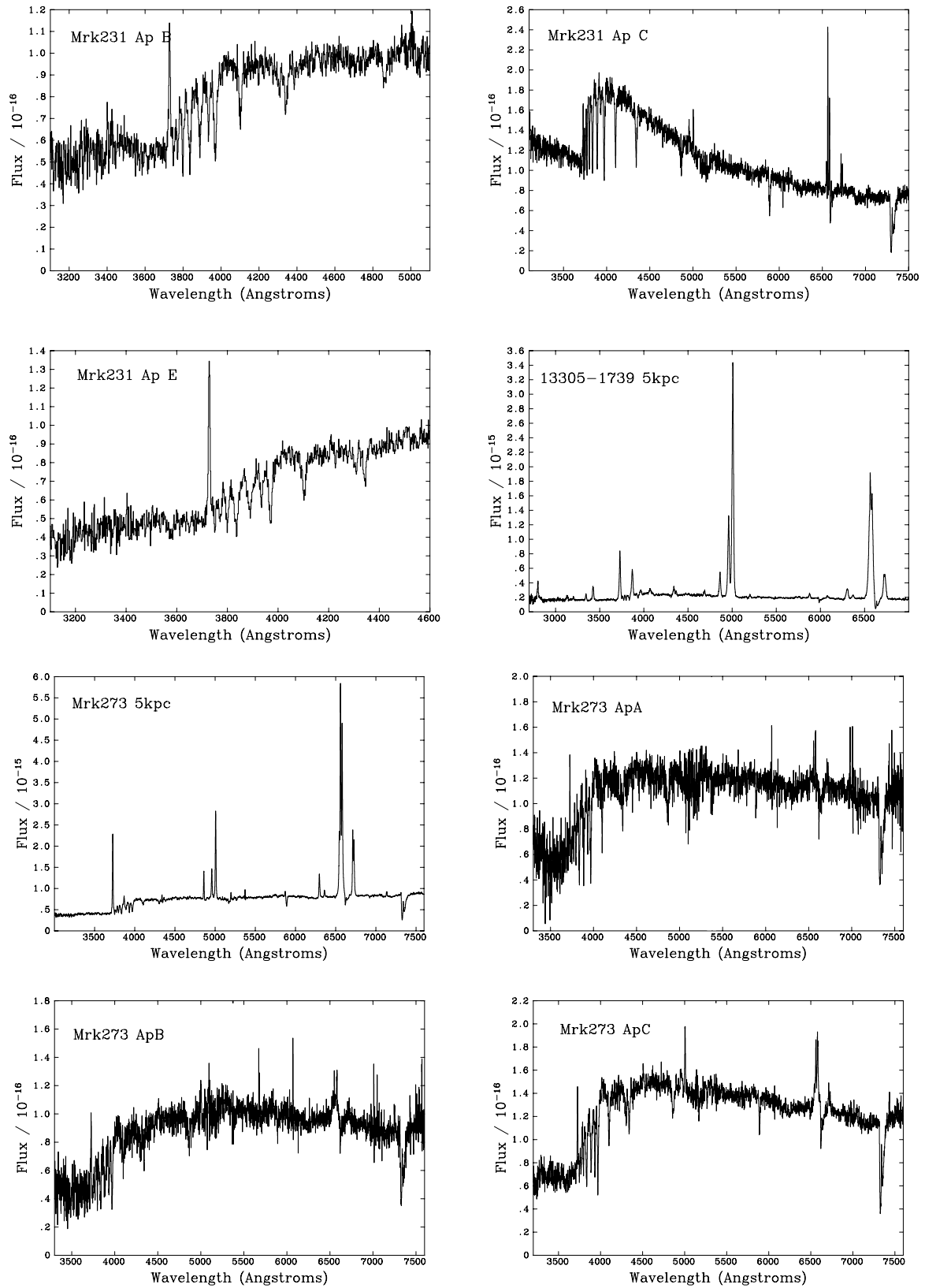
Figure 3 – *continued*
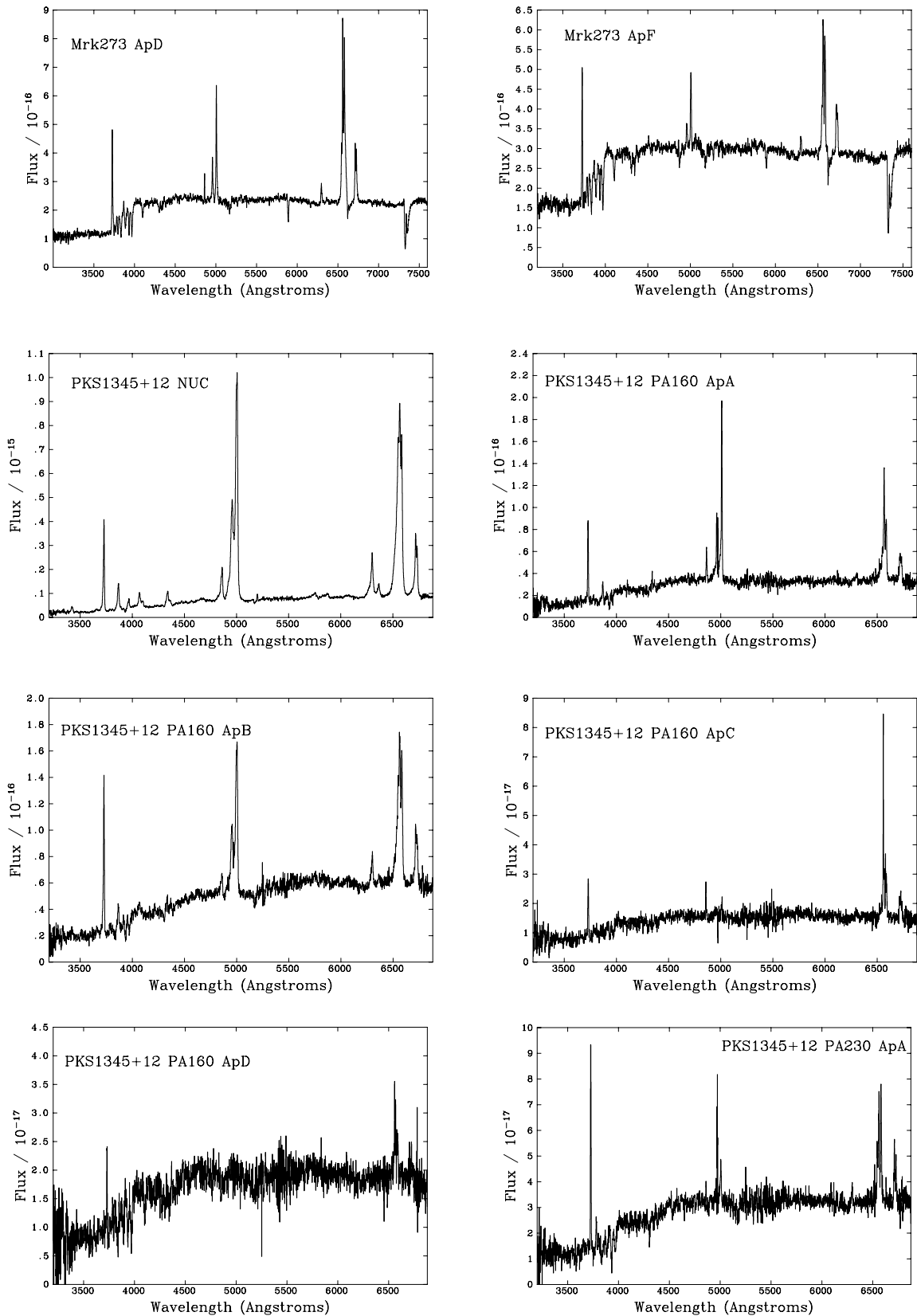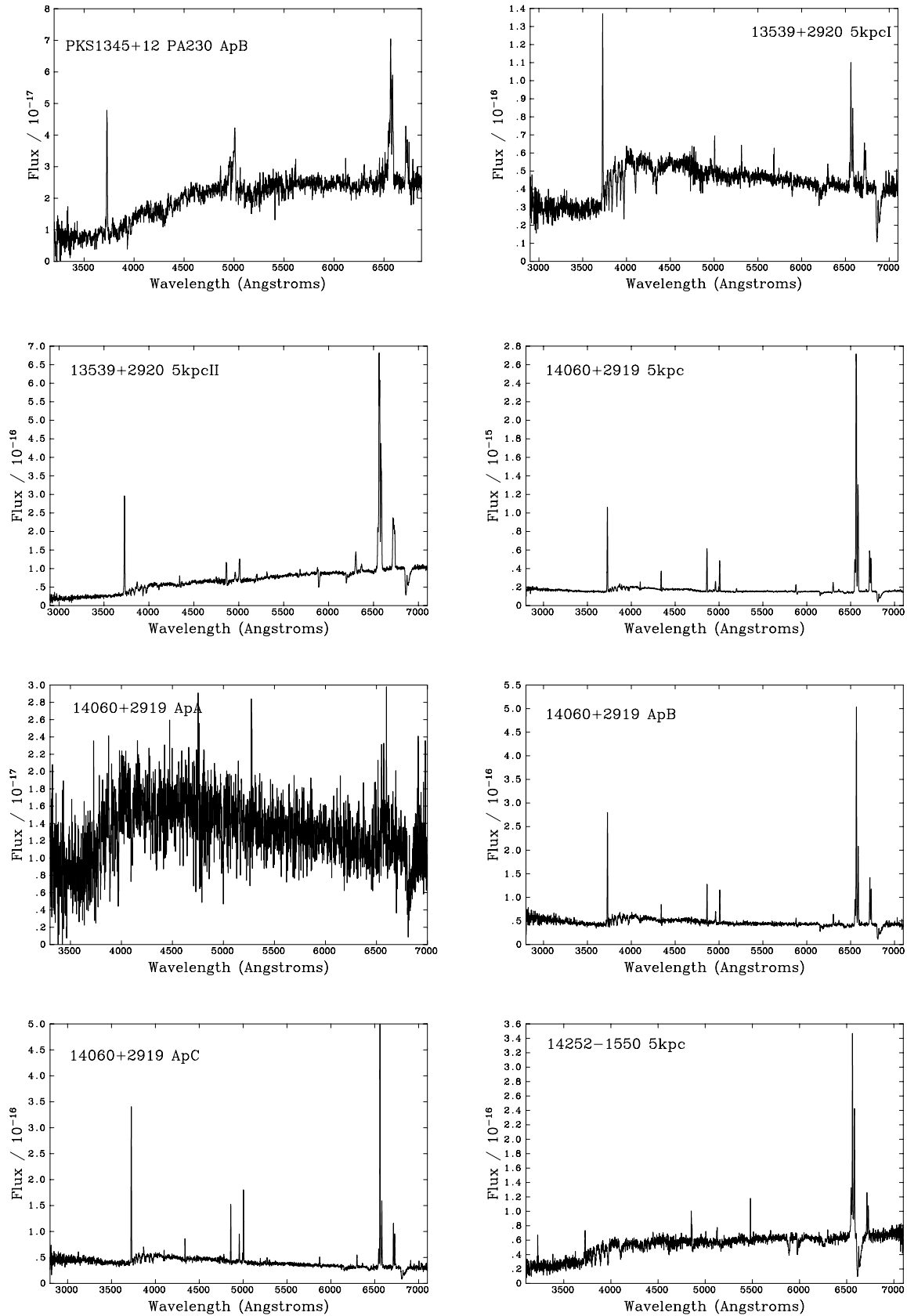
Figure 3 – *continued*

Figure 3 – *continued*

Figure 3 – *continued*
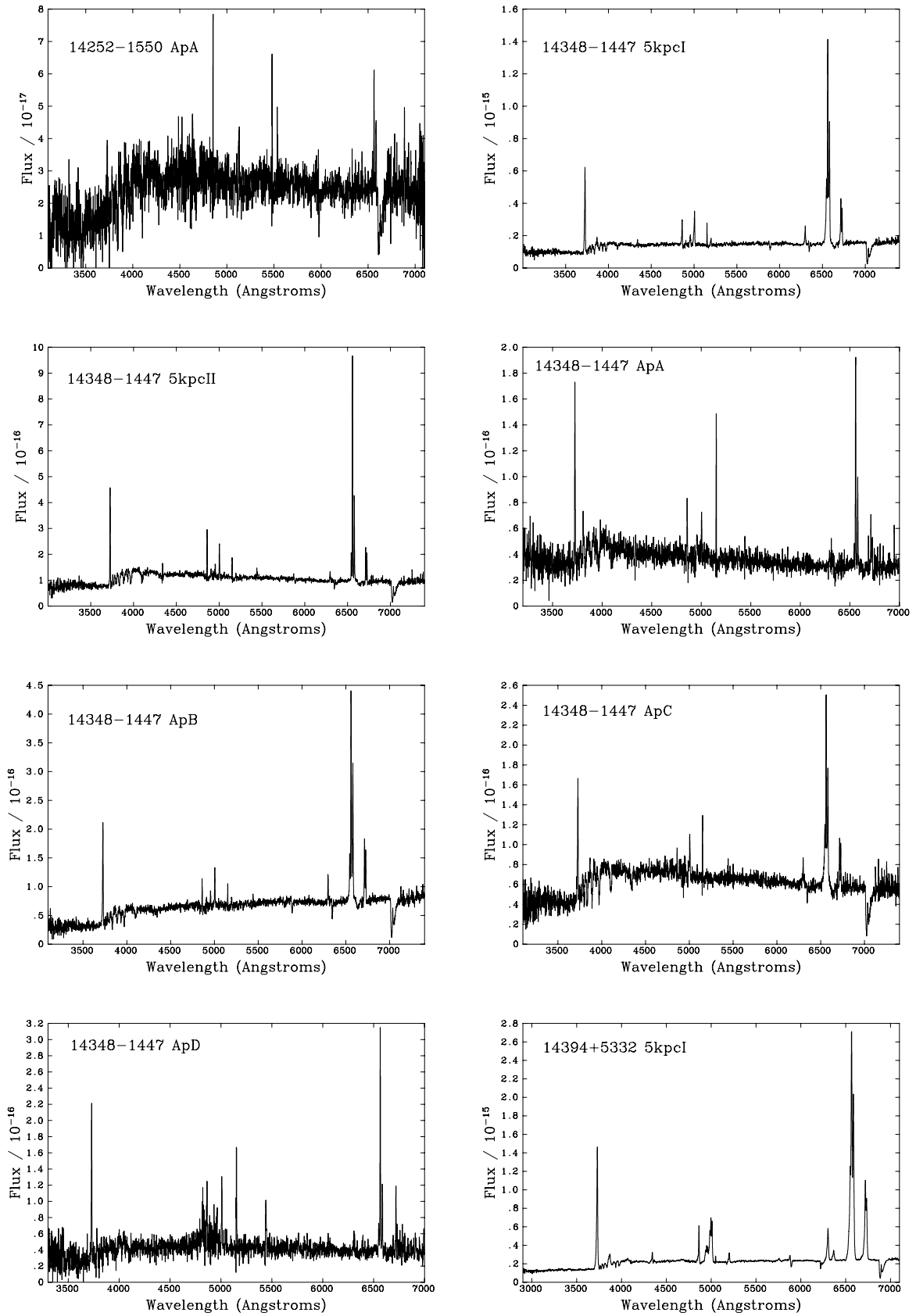
Figure 3 – *continued*
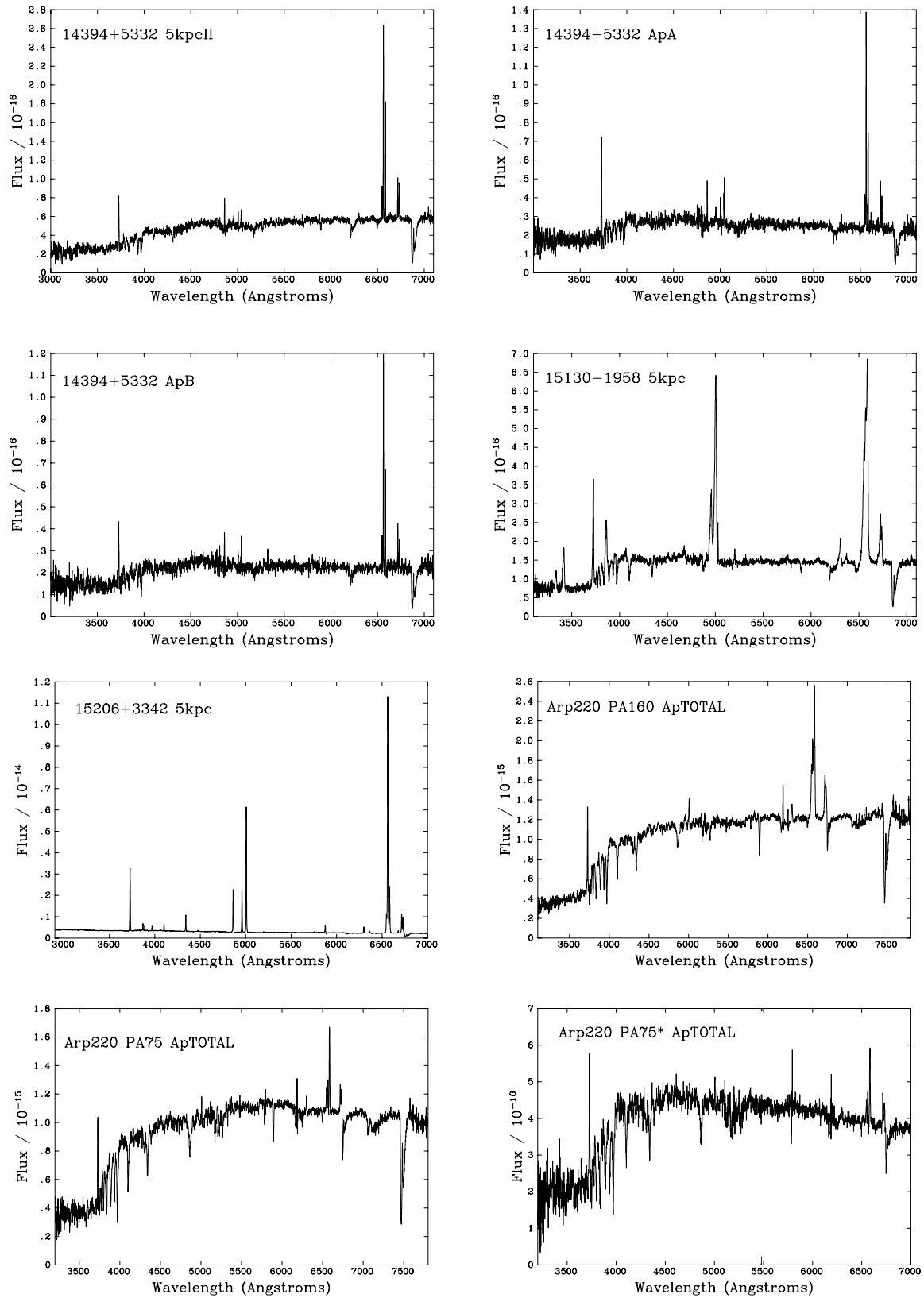
Figure 3 – *continued*
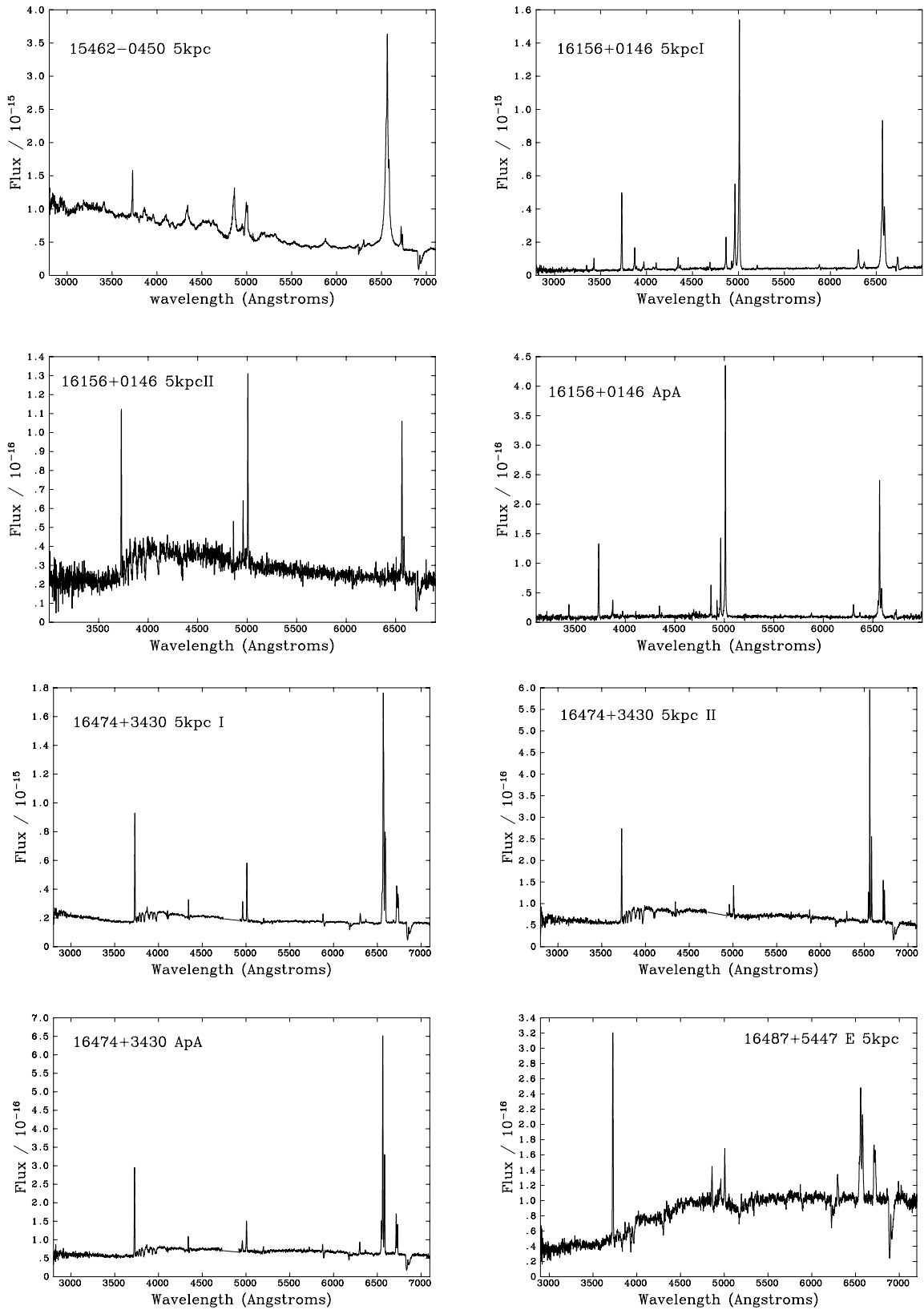
Figure 3 – *continued*
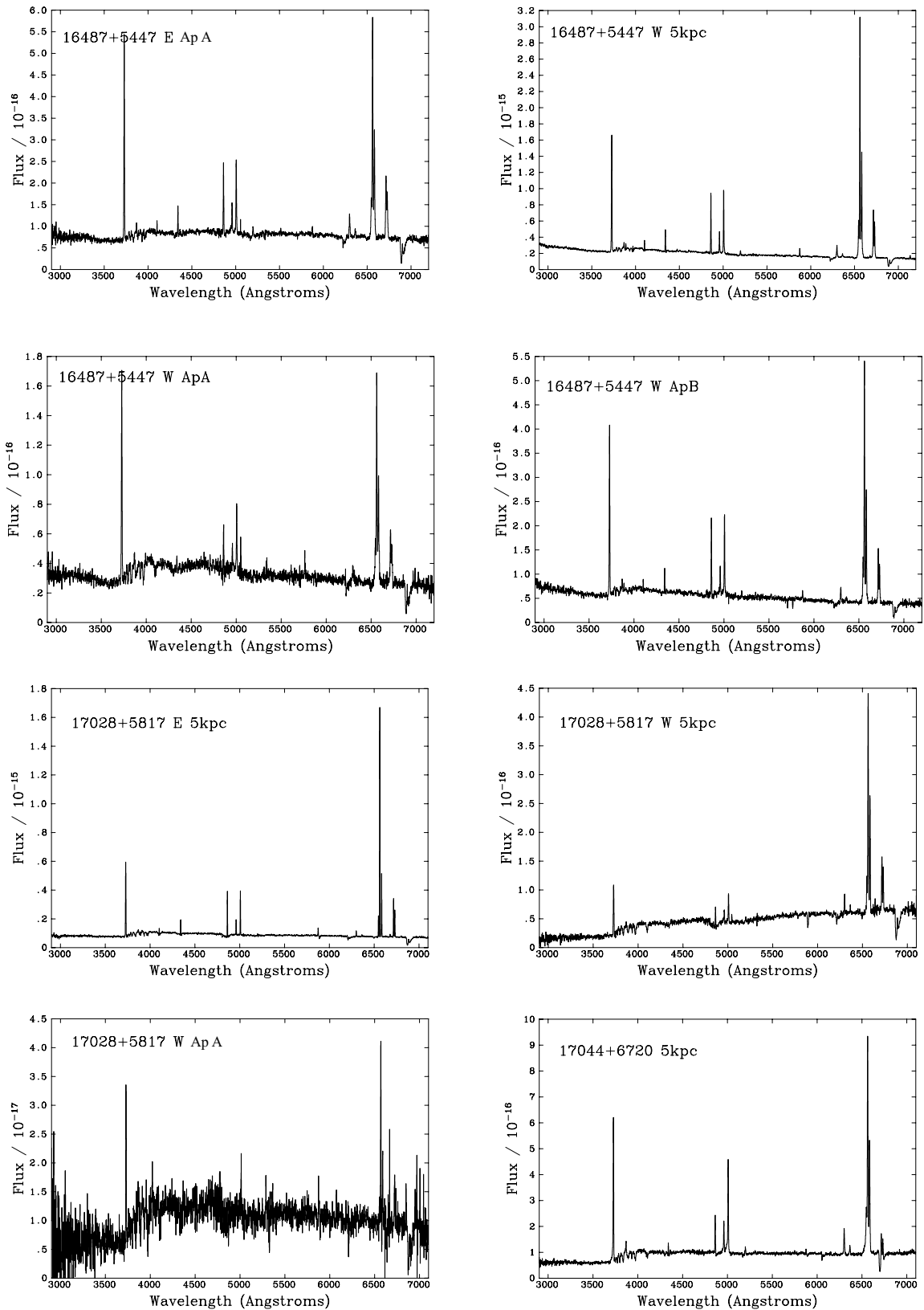
Figure 3 – *continued*
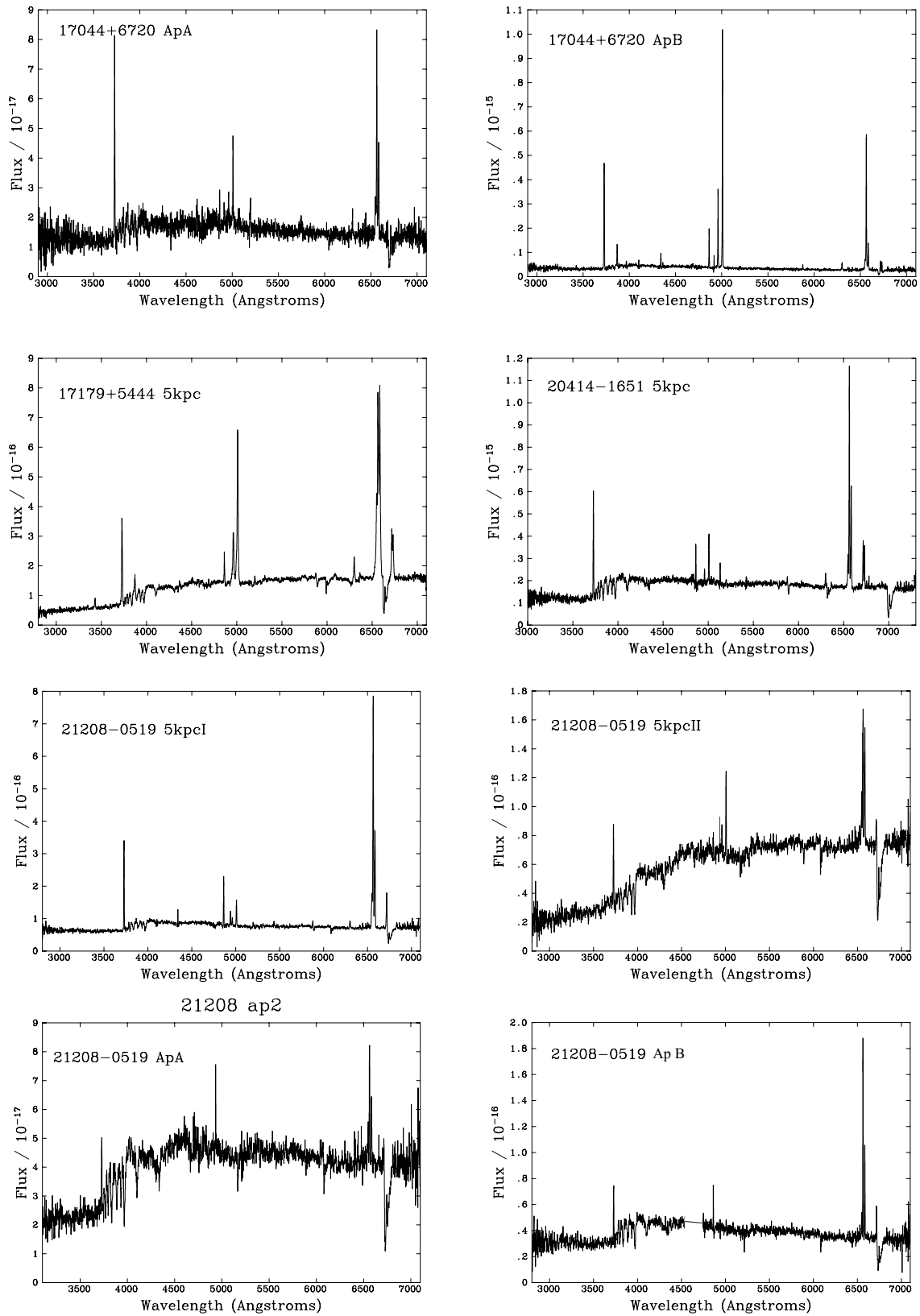
Figure 3 – *continued*

Figure 3 – *continued*
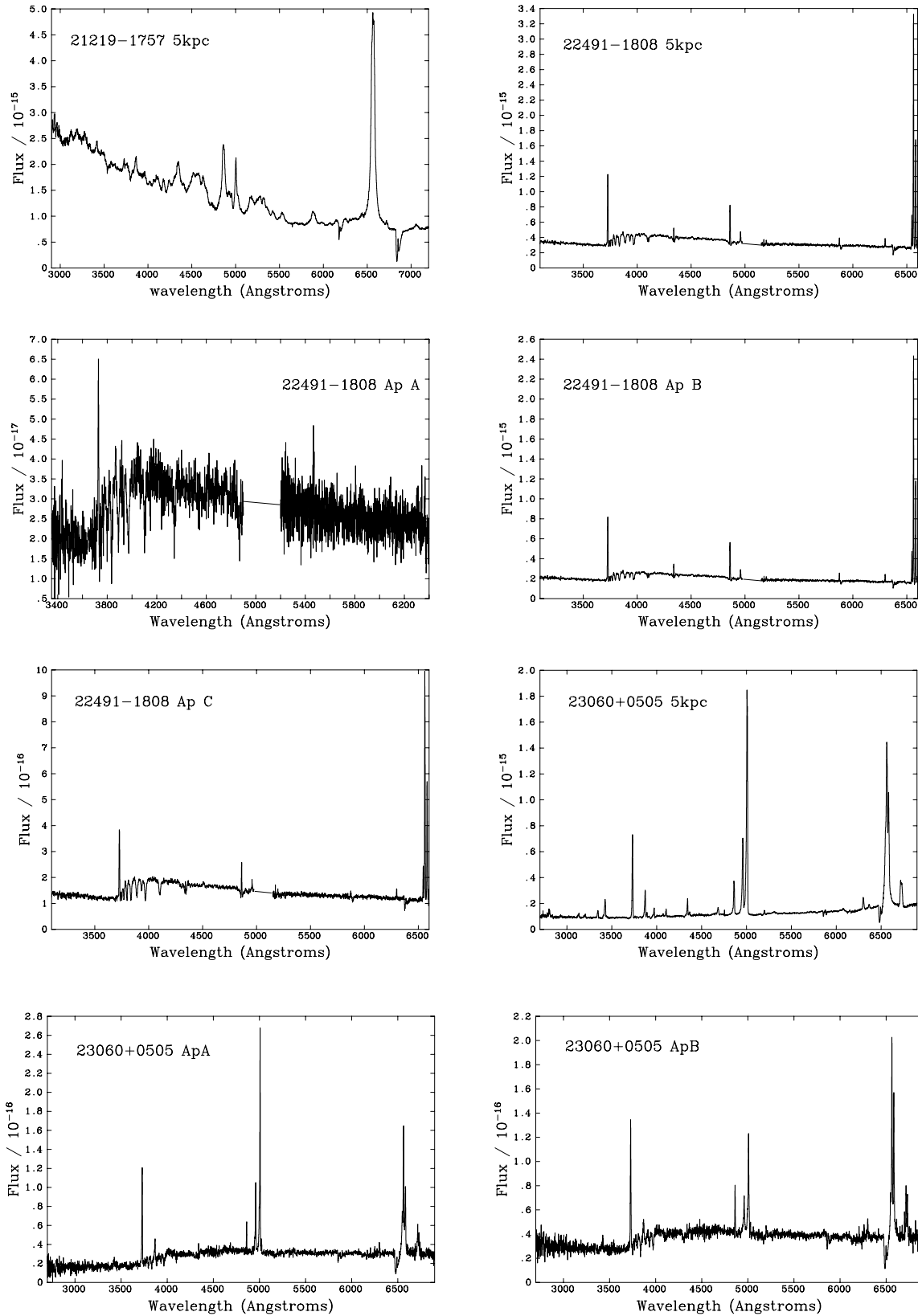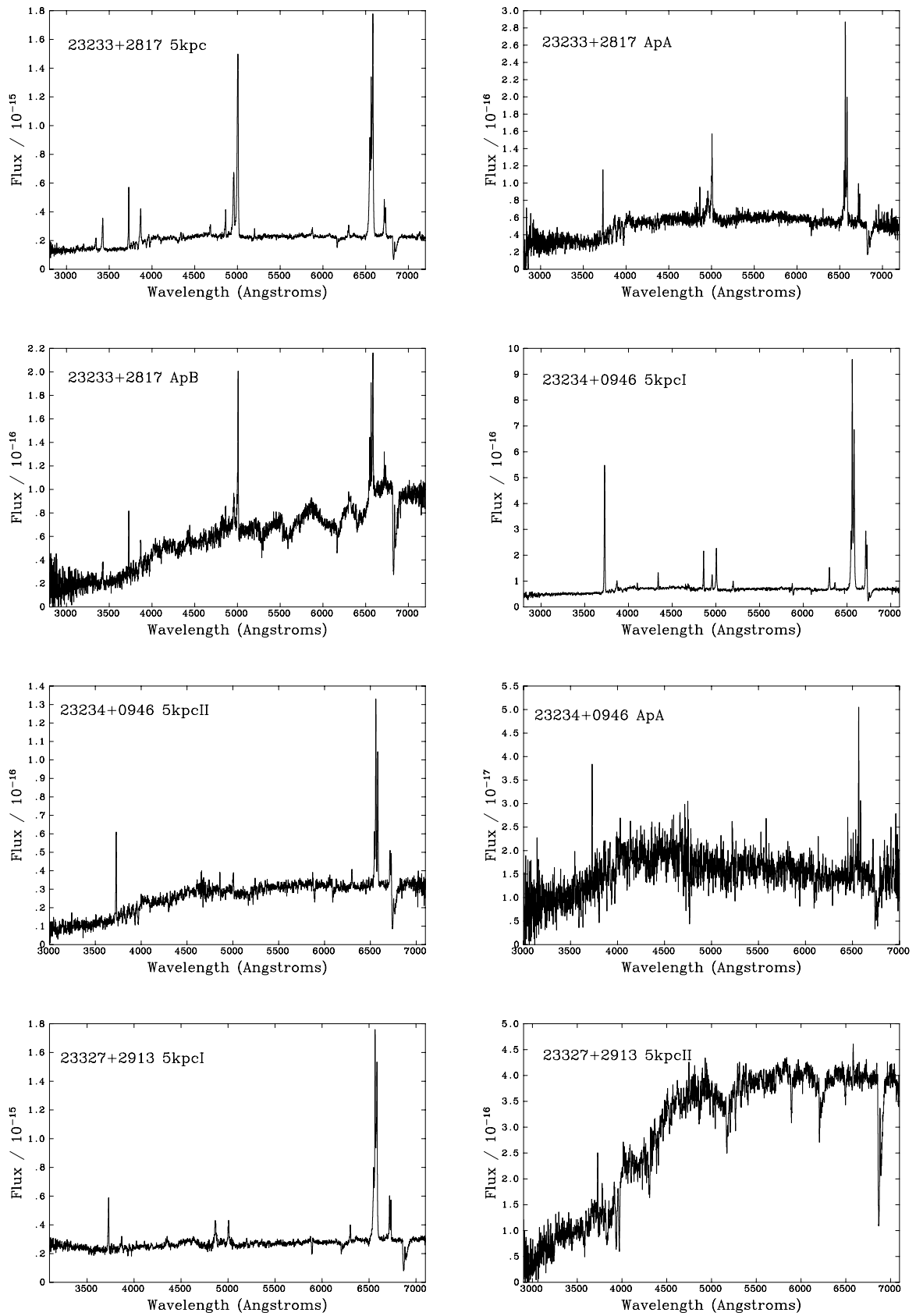
Figure 3 – *continued*
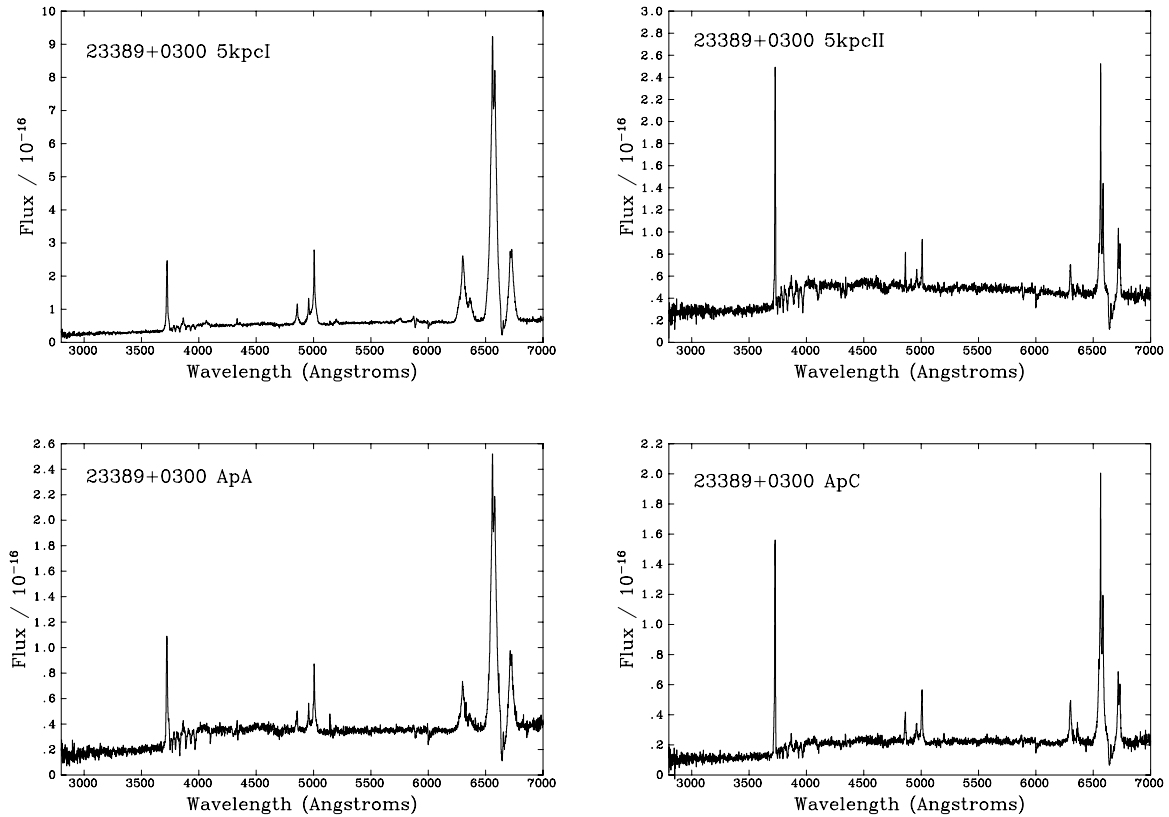
Figure 3 – *continued*

Figure 3 – *continued*

Fig. 2 shows the spatial profiles of the 2D frames in the wavelength range 4400–4600 Å along with the extraction apertures.

The extracted spectra, in the rest frame, are shown in Fig. 3. In the particular case of Arp 220 we extracted a total of 24 apertures. As discussed in RZ08, the morphologies of the extracted spectra (and the properties of the stellar populations) are similar across the entire extent of the galaxy. Therefore, in Fig. 3, we decided to show a representative sample of the whole set of extracted apertures. These are the apertures labelled as AP$_{\rm TOTAL}$ in Fig. 2 for each of the slit PAs used for this galaxy (see RZ08 for more details).

3.2 Modelling technique

To study in detail the properties of the stellar populations we have modelled the full spectral range of the extracted spectra using the stellar population synthesis model templates of Bruzual & Charlot (2003). These spectra were created assuming an instantaneous burst of star formation, solar metallicity and using the Salpeter (1955) initial mass function (IMF) with lower and upper mass cut-offs: $m_{\rm L} = 0.1\,{\rm M_\odot}$ and $m_{\rm U} = 100\,{\rm M_\odot}$ (see Tadhunter et al. 2005, for a justification of these assumption). Since ULIRGs have large gas and dust contents, it is important to carefully account for reddening effects. Reddened synthetic spectra were created using the Calzetti et al. (2000) reddening law, appropriate for starburst galaxies, and also the Seaton (1979) reddening law, representing the Galactic extinction case. During this process, the intrinsic extinction was modelled using a foreground screen geometry. Overall, there is good consistency between results obtained with the two reddening laws, suggesting that the main results for the ULIRGs in the CS and the ES samples are not sensitive to the details of the reddening law assumed at optical wavelengths.

Of the 133 extraction apertures, four sample the nuclear regions of type 1 Seyfert (Sy1) galaxies (5 kpc and Ap D for Mrk 231, 5 kpc for IRAS 15462−0405 and 5 kpc in the case of IRAS 21219−1757) and, therefore, it was not possible to model the extracted spectra due to the strong AGN contamination. In addition, Ap A for IRAS 23233+2817 samples a region to the south of the nucleus, including the bright knot detected in the *K*-band image shown in Kim et al. (2002, their fig. 1). Our extracted spectrum for this aperture shows that it is strongly contaminated by a Galactic M star (see Fig. 4). Therefore, no attempt was made to model the spectrum for this aperture.

Prior to the modelling, the spectra were corrected for Galactic reddening using the reddening law of Seaton (1979), along with $E(B - V)$ values derived from the far-IR-based maps of extinction by Schlegel, Finkbeiner & Davis (1998). An additional potential contaminant of the stellar emission in the optical is the nebular continuum emission (e.g. Dickson et al. 1995). In order to account for this effect, we subtracted a nebular continuum for those apertures for which strong emission lines were detected, following the technique described in RZ07, i.e. we used Hα to generate the nebular continuum and considered two extreme cases: (i) maximum nebular continuum assuming no reddening of the emission-line region; (ii) zero nebular continuum, corresponding to high reddening. The final nebular continua were subtracted from the spectra prior to performing the modelling. The modelling was carried out for both the nebular-corrected and uncorrected spectra.

Overall, a total of 128 extraction apertures were modelled. To perform the fit, we have used the CONFIT code (see Robinson et al. 2000; RZ08 for details) which assumes two stellar components plus a power-law in some cases. To summarize, the CONFIT approach consists of a direct fit to the overall continuum shape
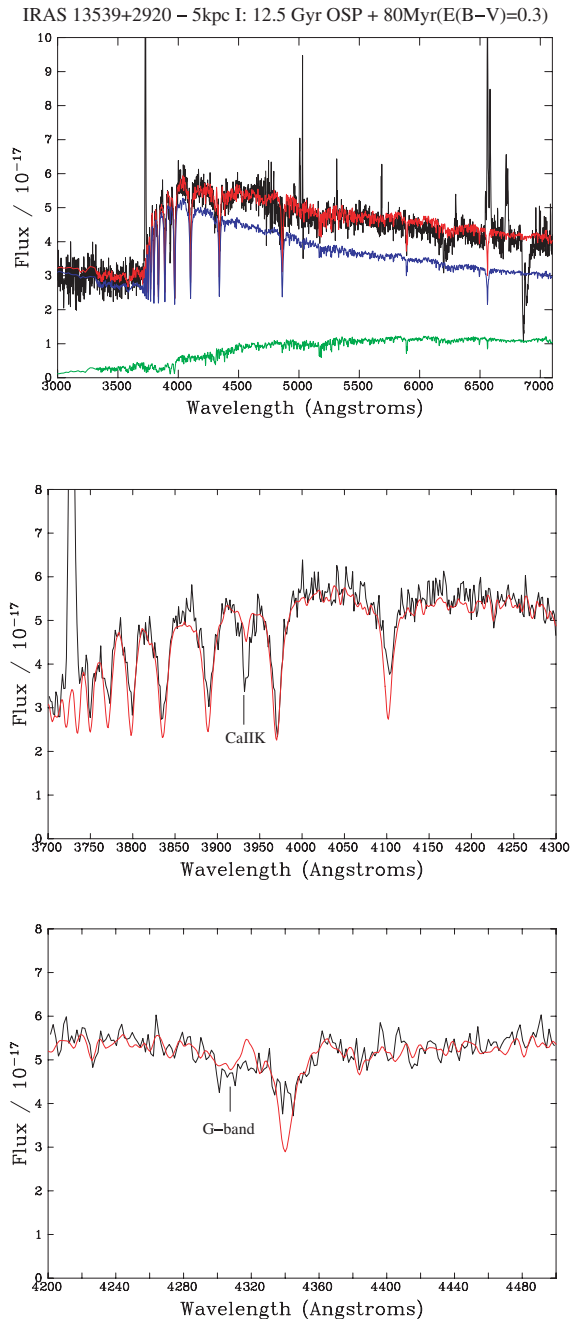
Figure 4. An example of the fits obtained using Comb I for the south-western nucleus (aperture 5 kpc I) in the case of IRAS 13539+2920. The model shown in the figure comprises a 12.5-Gyr OSP plus an 80-Myr VYSP [$E(B - V) = 0.3$] which contribute 17 and 79 per cent, respectively, to the flux in the normalizing bin (4600–4700 Å). The green, blue and red spectra correspond to the OSP, the VYSP and the sum of the two components, respectively. It is clear from the figure that the shape of the continuum is adequately fitted. However, the fit to the high-order Balmer lines and the *G*-band is not entirely satisfactory (although some overprediction is expected for the Balmer lines, since the spectrum shown in the figure has not been corrected for nebular emission). Moreover, there is a clear underprediction of the Ca II K absorption line.

of the extracted spectra using a minimum χ^2 technique. For each spectroscopic aperture, the flux is measured in several wavelength bins (typically ∼50–70) chosen to be as evenly distributed in wavelength as possible, and to avoid strong emission lines and atmospheric absorption features. A relative flux calibration uncertainty of ±5 per cent was assumed during the modelling. Models with $\chi^2_{red} \lesssim 1$ are deemed to provide an acceptable fit to the overall continua (see discussion in Tadhunter et al. 2005). From these, the best fitting models were selected based on a visual inspection of the fits to the detailed absorption features that have relatively little emission line contamination, such as high order Balmer lines, He I lines, Ca II K $\lambda3934$, *G*-band $\lambda4305$, Mg Ib $\lambda5173$ band. In addition, for those objects classified as H II galaxies, we used the Hα equivalent widths to further constrain the ages of the very young stellar population (VYSP).[4]

The model fit results are quantified in terms of the percentage contribution of the different stellar components in a normalizing bin. Because of the different spectral morphologies of the extracted spectra, it was not possible to select exactly the same normalizing bin for all the extracted apertures. However, the normalizing bin was always selected to be located within the wavelength range 4400–4800 Å, and usually extended ∼100 Å.

Since CONFIT allows for a maximum of two stellar components plus a power-law in some cases and the stellar contents of the galaxy are not known a priori, we used various combinations of spectra during the modelling process in order to determine the properties of the dominant stellar populations. We emphasize that the techniques and the modelling philosophy used in this paper are based on the results of RZ08 for the ULIRG Arp 220, and to a lesser extent on those of RZ07 for the case of PKS 1345+12.

Throughout this paper, we define *young stellar populations* (YSPs) as stellar components with ages $t_{YSP} \leq 2$ Gyr, and *old stellar populations* (OSP) as components with ages $t_{OSP} > 2$ Gyr. With the aim of better describing each combination, it is convenient to divide the YSPs into two groups:

(i) *VYSP*: stellar components with ages $t_{VYSP} \leq 0.1$ Gyr;

(ii) *intermediate-age young stellar populations* (IYSP): stellar components with ages in the range of $0.1 < t_{IYSP} \leq 2$ Gyr.

Generally, for models that include an old plus a young and/or an intermediate stellar component it is not possible to distinguish between OSP ages in the range $2 < t_{OSP} \leq 12$ Gyr, and therefore we decided not to use such stellar populations during the modelling analysis described below. Instead, we fixed the age of the OSP at 12.5 Gyr. The different combinations used during the modelling were as follows.

(i) *Combination I.* As a first approach we used a two component model comprising a YSP ($t_{YSP} \leq 2$ Gyr) with varying reddening [$0.0 \leq E(B - V) \leq 2.0$, increasing in steps of 0.1], along with an unreddened[5] OSP of age 12.5 Gyr. Accounting for an old component covers the case in which one or more of the merging galaxies is an early-type or bulge-dominated galaxy. It is worth mentioning that this combination is almost identical to the one used in RZ07 for the ULIRG PKS 1345+12. However, the version of the fitting code

---

[4] Note that since the continua of the spectra are affected by dilution due to the emission of older stellar components, the Hα equivalent width measurements provide upper limits for the age of the VYSP.

[5] Although we cannot entirely rule the idea that these stellar populations are significantly reddened, assuming zero reddening for OSP is reasonable, since such populations are likely to be situated in the extended bulge/halo in the foreground of the system (along the line of sight), or else completely obscured by the circumnuclear dust in the background of the system.

Table 4. Modelling results for the CS using Comb I (12.5 Gyr OSP + YSP). Column (1): object name. Column (2): aperture label as indicated in Fig. 2. Column (3): this column indicates whether or not Comb I fits both the overall shape of the continuum and the detailed absorption features: Y = yes, N = No. Column (4): range of ages for the YSP component that adequately fit the data ($\chi^2 \leq 1.0$). Column (5): range of $E(B - V)$ values of the YSPs in Column (4). Column (6): the percentage flux contribution of the YSP component to the model in the normalizing bin.

Object name IRAS (1)	Apertures (2)	Detailed features fitted? (3)	Age of YSP (Gyr) (4)	$E(B - V)$ (5)	Per cent YSP (6)
00091−0738	5 kpc	N	0.05–0.1	0.6	75–100
	Ap A	Y	0.2–1.0	0.0–0.1	45–50
	Ap B	Y	0.08–0.2	0.0–0.3	60–90
00188−0856	5 kpc	Y	0.3–0.5	0.4	80–100
01004−2237	5 kpc	Y	0.006–0.03	0.2–0.3	73–90
12072−0444	5 kpc	N	0.04–0.05	0.4–0.5	75–100
	Ap A	Y	0.1–0.3	0.0–0.1	50–65
	Ap B	N	0.06–0.1	0.0–0.2	60–95
12112+0305	5 kpc-I	N	0.04–0.06	0.6	∼100
	5 kpc-II	Y	0.06–0.1	0.0–0.1	65–70
	Ap A	N	0.05–0.06	0.6–0.7	80–85
12540+5708	5 kpc	–	–	–	
	Ap A	Y	0.005–0.007	0.1	∼40
	Ap B	Y	0.04–0.1	0.0–0.5	45–75
	Ap C	Y	0.07–0.08	0.1	95
	Ap D	–	–	–	
	Ap E	Y	0.06–0.1	0.2–0.5	50–70
13428+5608	5 kpc	N	0.05–0.06	0.5	∼75
	Ap A	Y	0.2–0.3	0.0	45–55
	Ap B	Y	0.08–0.2	0.0–0.1	35–40
	Ap C	N	0.09–0.2	0.0–0.3	45–60
	Ap D	N	0.07–0.1	0.1–0.3	50–75
	Ap E	N	0.05–0.06	0.5	∼75
	Ap F	N	0.05–0.1	0.0–0.4	40–55
13451+1232 (PA160)	5 kpc	Y	≤0.06	0.8–1.3	20–35
	Ap A	Y	0.1–0.2	0.0	25
			1.0–2.0	0.0	50–100
	Ap A neb	Y	0.2–1.2	0.0	20–80
	Ap B	Y	0.001–0.1	0.0–1.0	5–30
	Ap B neb	Y	0.004–0.4	0.0–1.0	10–20
	Ap C	Y	0.004–0.005	0.5–0.8	40–50
			0.04–0.1	0.0–0.3	30–50
	Ap D	Y	0.2–0.6	0.0–0.1	30–50
13451+1232 (PA230)	Ap A	Y	0.4–2.0	0.0–0.2	30–90
	Ap B	Y	≤2.0	0.0–1.0	10–90
13539+2920	5 kpc-I	N	0.07–0.2	0.0–0.3	65–100
	5 kpc-II	N	0.05–0.06	0.8	∼95
14060+2919	5 kpc	N	0.007	0.4	∼85
			0.03	0.3	∼85
	Ap A	Y	0.4–0.6	0.0	85–100
	Ap B	Y	0.03–0.04	0.3	88–100
	Ap C	Y	0.04–0.06	0.0–0.2	88–97
14348−1447	5 kpc-I	N	0.04–0.06	0.5	∼95
	5 kpc-II	Y	0.06–0.08	0.2–0.3	73–83
	Ap A	N	0.04–0.07	0.0–0.3	75–100
	Ap B	N	0.04–0.07	0.5–0.6	70–100
	Ap C	Y	0.06–0.2	0.0–0.3	70–75
	Ap D	Y	0.04–0.1	0.0–0.4	50–70
14394+5332	5 kpc-I	N	0.05–0.07	0.5	80–90
	5 kpc-II	Y	0.004–0.007	0.6–0.8	44–55
			0.04–0.06	0.4–0.5	50–55
	Ap A	Y	0.07–0.1	0.0–0.1	50–55
	Ap B	N	0.04–0.1	0.0–0.4	45–55
15130+1958	5 kpc	N	0.07–100	0.4–0.5	75–90
15206+3342	5 kpc	Y	0.01	0.3	91
15327+2340 (PA160)	5 kpc	N	0.07–0.1	0.8	∼70

Table 4 – *continued*

Object name IRAS (1)	Apertures (2)	Detailed features fitted? (3)	Age of YSP (Gyr) (4)	$E(B-V)$ (5)	Per cent YSP (6)
	Ap A	Y	0.4–0.6	0.0–0.1	60–85
	Ap B	Y	0.4–0.6	0.0	50–70
	Ap C	Y	0.4–0.6	0.4–0.5	50–90
	Ap D	N	0.05–0.1	0.9	~90
	Ap E	N	0.08–0.1	0.9	~75
	Ap F	Y	0.1–0.2	0.4–0.5	~60
	Ap G	Y	0.2–0.6	0.0–0.1	50–70
	Ap$_{\rm TOTAL}$	N	0.09–0.2	0.6	~70
15327+2340 (PA75)	Ap A	Y	0.2–0.6	0.1–0.4	50–95
	Ap B	Y	0.09–0.2	0.5	55–70
	Ap C	Y	0.2–0.3	0.5–0.6	~65
	Ap D	Y	0.2–0.4	0.3–0.4	55–75
	Ap E	Y	0.2–0.3	0.2–0.3	~60
	Ap F	Y	0.08–0.6	0.1–0.5	45–70
	Ap G	Y	0.05–0.6	0.1–0.5	45–80
	Ap$_{\rm TOTAL}$	Y	0.2–0.3	0.3–0.4	50–60
15327+2340 (PA75*)	Ap A	Y	0.2–0.6	0.0–0.1	50–95
	Ap B	Y	0.4–0.6	0.0–0.1	60–90
	Ap C	Y	0.4–0.6	0.0–0.1	70–100
	Ap D	Y	0.4–0.6	0.0–0.1	60–90
	Ap E	Y	0.4–0.8	0.0–0.1	50–100
	Ap F	Y	0.4–1.6	0.0–0.1	50–100
	Ap$_{\rm TOTAL}$	Y	0.2–0.6	0.0–0.1	45–85
16474+3430	5 kpc-I	N	0.007	0.4	85
	5 kpc-II	Y	0.07–0.08	0.1	70
	Ap A	Y	0.04	0.3	82
16487+5447 NE	5 kpc	Y	0.004–0.006	0.5–0.7	25–45
	Ap A	Y	0.004–0.007	0.3–0.5	55–70
16487+5447 NW	5 kpc	Y	0.005–0.007	0.2	75
	Ap A	N	0.05–0.09	0.0–0.2	55–75
	Ap B	Y	0.004–0.006	0.2–0.3	70–74
17028+5817 NE	5 kpc	N	0.04–0.08	0.0–0.3	70–90
17028+5817 NW	5 kpc	N	0.05–0.07	0.7	80–95
	Ap A	Y	0.2–0.6	0.0	70–100
20414−1651	5 kpc	N	0.07–0.1	0.1–0.4	65–90
21208−0519	5 kpc-I	N	0.004–0.005	0.6	80–90
			0.04–0.05	0.3	90–100
	5 kpc-II	Y	0.09–0.1	0.2–0.3	30–35
	Ap A	Y	0.1–0.2	0.0–0.2	~50
	Ap B	Y	0.1	0.0	65
22491−1808	5 kpc	N	0.04	0.3	100
	Ap A	N	0.05–0.1	0.0–0.3	65–100
	Ap B	N	0.04	0.2	87
	Ap C	N	0.05–0.07	0.1–0.2	80–90
23233+2817	5 kpc	Y	0.04–0.05	0.3–0.4	50–65
	Ap A	–	–	–	–
	Ap B	Y	0.06–0.1	0.1–0.3	50–60
23234+0946	5 kpc-I	N	0.006	0.6	88
			0.04	0.4	80
	5 kpc-II	Y	0.07–0.3	0.2–0.4	40–50
	Ap A	N	0.08–0.2	0.0–0.3	60–75
23327+2913	5 kpc-I	Y	0.009	0.3–0.4	51–66
	5 kpc-II	Y	≤2	≤2.0	≤50
	Ap A	Y	0.009	0.3–0.4	51–66
	Ap B	Y	≤2	≤2.0	≤50

used here represents an updated version of the one used in that paper. Therefore, in order to compare the results obtained or this galaxy with those of the other ULIRGs in our sample, we decided to model again the extracted spectra for PKS 1345+12 using this combination

and the updated version of the code. The results obtained here are consistent with those of RZ07. For consistency, the spectra of this source were also modelled using the other two combinations described below.

Table 5. Same as Table 4 but for the 10 additional ULIRGs included in the ES.

Object name IRAS (1)	Apertures (2)	Detailed features fitted? (3)	Age of YSP (Gyr) (4)	$E(B-V)$ (5)	Per cent YSP (6)
08572+3915	5 kpc	N	0.06–0.1	0.0–0.3	65–90
	Ap A	Y	0.1–0.3	0.0–0.1	45–55
	Ap B	N	0.07–0.1	0.0–0.2	60–85
	Ap C	Y	0.07–0.1	0.2–0.3	90–100
10190+1322	5 kpc-I	N	0.05–0.08	0.3–0.5	65–90
	5 kpc-II	N	0.2	0.5	85
	Ap A	Y	0.4–0.7	0.0–0.2	60–95
	Ap B	N	0.04–0.06	0.5–0.6	80–95
10494+4424	5 kpc	N	0.07–0.1	0.7	95–100
	Ap A	Y	0.4	0.0–0.1	72–87
	Ap B	N	0.04–0.1	0.0–0.4	75–100
13305−1739	5 kpc	N	0.05–0.1	0.0–0.4	65–90
14252−1550	5 kpc	N	0.05–0.1	0.5–0.6	80–85
	Ap A	Y	0.2–0.7	0.0–0.2	50–100
16156+0146	5 kpc-I	Y	0.01	0.5	75
	5 kpc-II	N	0.08–0.1	0.1–0.3	75–98
	Ap A	Y	0.004–0.007	0.3–0.5	40–80
			0.03–0.04	0.1–0.3	50–75
17044+6720	5 kpc	Y	0.05–0.08	0.4	80–85
	Ap A	Y	0.05–0.1	0.0–0.3	70–90
	Ap B	N	0.05–0.1	0.0–0.2	77–95
17179+5444	5 kpc	N	0.07–0.1	0.4–0.6	50–85
23060+0505	5 kpc	N	–	–	–
	Ap A	Y	0.05–0.1	0.1–0.4	43–65
	Ap B	Y	0.04–0.06	0.2–0.3	65
23389+0303	5 kpc-I	N	0.004	0.9	∼100
			0.04	0.6	90
	5 kpc II	N	0.07–0.1	0.2–0.4	70–85
	Ap A	N	0.06	0.5	85
	Ap B	N	0.005–0.006	0.8–0.9	85
	Ap C	N	0.05–0.08	0.4	63–76
	Ap D	N	0.1	0.2	72

(ii) *Combination II.* This combination consists of three components: an OSP of age 12.5 Gyr and zero reddening, along with a YSP with variable reddening [$0.0 \leq E(B-V) \leq 2.0$, increasing in steps of 0.1], and a power-law ($F_\lambda \propto \lambda^\alpha$) with a spectral index in the range $-15 < \alpha < 15$. The power-law is included to represent either scattered or direct AGN continuum component (Tadhunter et al. 2002), or a highly reddened VYSP.

(iii) *Combination III.* For ULIRGs as a class, there is no reason, a priori, to expect a large contribution to the optical emission from a 12.5-Gyr OSP. Therefore, in order to explore the possibility of YSPs dominating the optical light from the objects in our sample, we used a combination of two YSP components: a IYSP with ages in the range 0.3–2.0 Gyr, and $E(B-V)$ values of 0.0, 0.2 or 0.4, plus a VYSP with age in the range 1-100 Myr and reddening [$0.0 \leq E(B-V) \leq 2.0$, increasing in steps of 0.1]. Note that for this combination, we assume that the IYSPs have relatively low reddening [$E(B-V) \leq 0.4$].

The modelling results found for all the ULIRGs in the CS and the ES are shown in Tables 4–9 for Combination I, Combination II and Combination III (hereafter Comb I, Comb II and Comb III). For the majority of the objects in our sample, the nebular correction mentioned before did not lead to a significant change in the modelling results for any of the combinations, and the uncertainties in the ages, reddenings and percentage contributions presented in

the tables already account for such minor changes. Therefore, we show only the results for zero nebular correction in the tables for all objects with the exception of PKS 1345+12. For this galaxy, we subtracted the best model for the nebular continuum emission from the work of Holt et al. (2003), in the case of the 5-kpc aperture. The nebular emission is also important for Ap A and to a lesser extent Ap B. For these two apertures, both the nebular corrected and uncorrected results are shown in Table 4. We now give a general overview of the results obtained for Comb I, Comb II and Comb III.

4 MODELLING RESULTS

4.1 Combination I

In the case of Comb I, adequate fits ($\chi^2 \leq 1.0$) to the overall shape of the spectral energy distribution (SED) were obtained for all the extraction apertures modelled, with the exception of the 5-kpc aperture in IRAS 23060+0505, for which a power-law is required. However, although this combination fits the overall shape of the continuum, it fails to fit the absorption features (high-order Balmer lines, Ca II K, G-band) for ∼42 per cent (54) of the extraction apertures modelled. Fig. 4 shows a representative example of the fits obtained using this combination. The aperture selected for the figure samples the south-eastern nucleus (5 kpc-I) of IRAS 13539+2920. The figure shows the best-fitting model to both the continuum and the detailed

Table 6. Modelling results for the CS using Comb II (OSP + YSP + power-law). Column (1): object name. Column (2): aperture label as indicated in Fig. 2. Column (3): range of ages for the YSP components that adequately fit the data (both the continuum and the detailed features). Column (4): range of $E(B-V)$ values of the YSPs in Column (3). Column (5): the percentage flux contribution of the YSP component to the model, in the normalizing bin. Columns (6) and (7): same as Column (5) for the power-law and OSP, respectively.

Object name IRAS	Aperture	Age of YSP (Gyr)	$E(B-V)$	Per cent YSP	Per cent power-law	Per cent OSP
(1)	(2)	(3)	(4)	(5)	(6)	(7)
00091−0738	5 kpc	0.3–0.6	0.0–0.2	48–60	20–35	5–30
	Ap A	0.4–1.0	0.0–0.3	50–100	6–12	≤25
	Ap B	0.2–0.6	0.0–0.2	66–75	10–25	≤24
00188−0856	5 kpc	0.3–0.6	0.3–0.4	75–90	8–10	≤16
01004−2237	5 kpc	0.03–0.1	0.0–0.5	30–50	∼40	10–30
12072−0444	5 kpc[1]	–	–	–	–	–
	Ap A	0.2–0.6	0.0–0.2	40–65	7–30	≤50
	Ap B	0.5–0.6	0.0	50–60	40	≤10
12112+0305	5 kpc I	0.4–0.5	0.0–0.1	50–60	∼40	≤10
	5 kpc II	0.2–0.5	0.0–0.2	50–60	30–40	≤15
	Ap A	0.2–0.8	0.0–0.1	40–70	20–40	≤45
12540+5708	5 kpc	–	–	–	–	–
	Ap A	0.4–1.4	0.1–0.5	40–75	25–40	≤35
	Ap B	0.2	0.0	40	30	30
	Ap C	0.09–0.2	0.0–0.1	70–88	10–30	0
	Ap D	–	–	–	–	–
	Ap E	0.1–0.2	0.0–0.1	30	40	30
13428+5608	5 kpc	0.5–0.8	0.0–0.1	45–60	∼40	≤15
	Ap A	0.4–0.8	0.0–0.3	50–85	10–15	≤35
	Ap B	0.2–0.7	0.0–0.2	33–64	6–15	30–65
	Ap C	0.4–0.7	0.0–0.2	50–90	6–9	≤45
	Ap D	0.5–0.8	0.0–0.3	50–80	18–23	≤30
	Ap E	0.5–0.8	0.0–0.1	40–60	∼40	≤20
	Ap F	0.5–0.7	0.0–0.4	45–80	15–30	≤30
13451+1232 (PA160)	5 kpc[3]	–	–	–	–	–
	Ap A	0.2–0.8	0.0–0.2	20–35	∼5	60–75
	Ap B[3]	–	–	–	–	–
	Ap C	0.4–0.8	0.0–0.3	35–75	15–25	5–45
	Ap D	0.4–1.2	0.0–0.5	30–85	10–16	≤45
13451+1232 (PA230)	Ap A	0.5–1.4	0.0–0.5	40–90	3–10	≤50
	Ap B	0.4–1.0	0.0–0.2	25–50	5–10	45–65
13539+2920	5 kpc-I	0.5–0.6	0.0–0.2	65–80	20–30	0
	5 kpc-II	0.5–0.8	0.2–0.5	50–70	35–40	≤15
14060+2919	5 kpc	0.004	0.5	93	6	0
	Ap A	0.3–0.8	0.0–0.4	60–90	10–15	≤25
	Ap B	0.04–0.06	0.0–0.4	60–85	10–25	≤10
	Ap C	0.2–0.3	0.0	50	40	11
14348−1447	5 kpc-I[1]	–	–	–	–	–
	5 kpc-II	0.5	0.0	62	38	0
	Ap A	0.1–0.3	0.0–0.1	40–50	40	10–20
	Ap B	0.2–0.6	0.0–0.1	30–40	30–40	12–40
	Ap C	0.09–0.4	0.0–0.4	45–80	5–35	≤35
	Ap D	0.05–0.4	0.0–0.5	40–75	5–30	≤50
14394+5332	5 kpc-I[1]	–	–	–	–	–
	5 kpc-II	0.7–2.0	0.0–0.2	40–70	30–35	≤30
	Ap A	0.3–0.8	0.0–0.2	42–60	30–35	≤25
	Ap B	0.4–1.0	0.0–0.3	40–60	23–35	≤30
15130+1958	5 kpc	0.2–0.5	0.0–0.2	55–70	∼30	≤15
15206+3342	5 kpc[2]	–	–	–	–	–
15327+2340 (PA160)	5 kpc	0.4–0.7	0.4–0.5	64–85	15–18	≤20
	Ap A	0.5–0.7	0.0–0.1	75–98	∼2	≤20
	Ap B	0.5–0.7	0.1–0.2	85–95	3–5	≤20
	Ap C	0.4–0.7	0.3–0.5	70–98	4–5	≤20
	Ap D	0.4–0.6	0.5–0.8	62–75	27–35	≤8
	Ap E	0.4–0.6	0.6–0.8	75–85	10–16	≤15
	Ap F	0.1–0.7	0.2–0.4	53–85	4–17	≤43
	Ap G	0.4–0.7	0.0–0.2	55–90	4–8	≤40
	Ap$_{TOTAL}$	0.3–0.7	0.2–0.4	48–87	5–15	≤45

Table 6 – *continued*

Object name IRAS (1)	Aperture (2)	Age of YSP (Gyr) (3)	$E(B-V)$ (4)	Per cent YSP (5)	Per cent power-law (6)	Per cent OSP (7)
15327+2340 (PA75)	Ap A	0.3–0.7	0.1–0.3	60–93	3–7	≤37
	Ap B	0.2–0.6	0.2–0.5	50–75	6–18	10–44
	Ap C	0.3–0.6	0.4–0.5	65–85	6–12	8–27
	Ap D	0.3–0.7	0.2–0.4	61–95	3–9	≤37
	Ap E	0.3–0.7	0.1–0.4	52–85	4–10	9–45
	Ap F	0.3–0.9	0.1–0.5	30–85	2–13	10–70
	Ap G	0.2–1.0	0.0–0.3	38–90	7–16	≤60
	Ap$_{TOTAL}$	0.2–0.6	0.2–0.4	57–75	4–12	12–40
15327+2340 (PA75*)	Ap A	0.3–0.6	0.0–0.2	55–90	3–10	≤40
	Ap B	0.4–0.7	0.0–0.2	59–95	2–5	≤41
	Ap C	0.4–0.6	0.0–0.2	63–90	4–8	≤33
	Ap D	0.4–0.7	0.0–0.2	55–90	7–10	≤40
	Ap E	0.4–1.2	0.0–0.3	40–90	9–11	≤52
	Ap F	0.5–1.6	0.0–0.3	45–95	2–10	≤48
	Ap$_{TOTAL}$	0.4–0.7	0.0–0.3	51–93	7–9	≤45
16474+3430	5 kpc-I[a]	–	–	–	–	–
	5 kpc-II	0.2–0.4	00–0.2	50–65	20–30	≤25
	Ap A[b]	–	–	–	–	–
16487+5447 NE	5 kpc	0.5–1.0	0.1–0.3	30–50	10–15	40–60
	Ap A	0.04–0.1	0.0–0.3	25–45	15–33	33–40
16487+5447 NW	5 kpc[a]	0.04	0.2	60	30	10
	Ap A	0.2–0.4	0.0–0.1	48–55	16–20	25–30
	Ap B	0.04–0.3	0.0–0.2	50–66	10–35	20–40
17028+5817 NE	5 kpc[b]	–	–	–	–	–
17028+5817 NW	5 kpc	0.3–0.6	0.1–0.4	50–60	25–35	10–25
	Ap A	0.3–0.6	0.0	64–75	16–20	≤15
20414−1651	5 kpc	0.3–0.6	0.0–0.2	50–65	20–40	≤15
21208−0519	5 kpc-I	0.1–0.2	0.0–0.2	45–50	30–40	10–25
	5 kpc-II	0.2–1.2	0.0–0.5	25–85	10–22	≤65
	Ap A	0.2–0.6	0.0–0.2	46–70	5–20	10–50
	Ap B	0.2–0.6	0.0–0.1	47–55	25–35	10–22
22491−1808	5 kpc[a]	–	–	–	–	–
	Ap A	0.4–0.6	0.0–0.2	67–85	15–30	0
	Ap B[a]	–	–	–	–	–
	Ap C[a]	–	–	–	–	–
23233+2817	5 kpc	0.05–0.5	0.0–0.3	25–45	15–40	20–40
	Ap A	–	–	–	–	–
	Ap B	0.07–0.4	0.0–0.3	35–44	6–20	40–50
23234+0946	5 kpc-I	0.04–0.2	0.0–0.4	20–63	17–40	20–40
	5 kpc-II	0.1–1.0	0.0–0.4	35–80	5–20	≤60
	Ap A	0.5–0.8	0.0	65–85	10–20	≤15
23327+2913	5 kpc-I	0.001–0.003	0.5	40–45	25–35	25
		0.01	0.1	30	40	30
	5 kpc-II[c]	–	–	–	–	–
	Ap A	0.001–0.003	0.5	40–45	25–35	25
		0.01	0.1	30	40	30
	Ap B[c]	–	–	–	–	–

[a]No adequate fits (fitting both the continuum and the detailed absorption features) are found using Comb II.

[b]No adequate fits are found with a non-negligible contribution of the power-law component (i.e. different than those of Comb I) and therefore, no results are presented in the table.

[c]When a power-law is included, adequate fits are found for the entire range of YSP combinations used and, therefore, no results are presented in the table.

absorption features, obtained for that aperture. It is clear from the figure that Comb I fits the optical continuum SED adequately, but there is an underprediction of the Ca II K absorption feature and, also, the fit to the Balmer lines and the *G*-band is not entirely satisfactory. This result suggests that the simple Comb I models may not be adequate for modelling the detailed absorption features for a subset of the ULIRGs in our sample. However, note that, the greatest disagreement between the Comb I fits and the data often occurs for

the Ca II K line, which potentially has a contribution from absorption by the interstellar medium (ISM) in the host galaxy.[6] Therefore, for many of the 42 per cent without adequate fits to the absorption lines,

[6] ~46 per cent of the apertures for which Comb I does not perfectly fit the Ca II K absorption feature show a strong Na I D absorption feature. The Na I D line is also potentially affected by the ISM of the host galaxy.

Table 7. Same as Table 6, but for the 10 additional ULIRGs included in the ES.

Object name IRAS	Aperture	Age of YSP (Gyr)	$E(B-V)$	Per cent YSP	Per cent power-law	Per cent OSP
(1)	(2)	(3)	(4)	(5)	(6)	(7)
08572+3915	5 kpc	0.2–0.6	0.0–0.2	60–70	30–36	≤25
	Ap A	0.2–0.6	0.0–0.3	50–85	5–20	≤45
	Ap B	0.4	0.0–0.1	65–75	25–30	0
	Ap C	0.09–0.4	0.0–0.3	73–95	6–35	≤12
10190+1322	5 kpc-I[a]	–	–	–	–	–
	5 kpc-II[a]	–	–	–	–	–
	Ap A	0.4–0.7	0.0–0.2	70–95	~5	≤25
	Ap B[a]	–	–	–	–	–
10494+4424	5 kpc[a]	–	–	–	–	–
	Ap A[b]	–	–	–	–	–
	Ap B	0.07–0.2	0.0–0.2	65–85	10–40	≤10
13305−1739	5 kpc	0.3–0.5	0.0–0.2	50–60	40	≤10
14252−1550	5 kpc	0.2–0.6	0.0–0.2	40–66	15–35	≤35
	Ap A	0.2–0.8	0.0–0.2	60–85	10–20	≤45
16156+0146	5 kpc-I	≤0.03	0.2–0.7	25–55	30–40	14–40
	5 kpc-II	0.4–0.5	0.0–0.1	70–80	20–26	0
	Ap A	0.05–1.0	0.2–0.5	15–66	30–40	≤30
17044+6720	5 kpc	0.2–0.4	0.0–0.1	~50	36–40	10–15
	Ap A	0.2–0.7	0.0–0.2	50–62	35–40	≤15
	Ap B	0.4–0.5	0.0	55	40	5
17179+5444	5 kpc	0.2–0.6	0.1–0.3	40–62	22–35	6–50
23060+0505	5 kpc	0.01	0.4	72	6	22
	Ap A	0.07–0.6	0.0–0.3	35–50	6–30	20–35
	Ap B	0.05–0.6	0.0–0.4	40–60	8–35	5–30
23389+0303	5 kpc-I[a]	–	–	–	–	–
	5 kpc-II	0.2–0.7	0.0	53–70	12–30	≤35
	Ap A	0.4–0.6	0.0–0.1	~60	~40	0
	Ap B[a]	–	–	–	–	–
	Ap C	0.5–0.8	0.0–0.1	50–70	~30	≤20
	Ap D	0.2–0.5	0.0–0.1	55–65	10–30	2–30

[a]No adequate fits (fitting both the continuum and the detailed absorption features) are found using Comb II.
[b]No adequate fits are found with a non-negligible contribution of the power-law component (i.e. different than those of Comb I) and therefore, no results are presented in the table.

it is difficult to rule out the idea that Comb I provides adequate fits to the stellar continuum.

Overall, even if the Comb I fits are not always perfect, they give single-valued estimates of the luminosity-weighted age, reddening and percentage contribution of the YSPs within each aperture. Therefore, the results of Comb I – presented in Tables 4 and 5 – are still useful when performing a statistical analysis of the results.

4.2 Combination II

For those ULIRGs in our sample also classified as Sy2 galaxies, it is possible that the optical spectrum is a composite of stellar and AGN continuum emission (e.g. scattered light or weak direct AGN light; see Tadhunter et al. 2002). In this context, we note that significant starburst activity has already been detected in the nuclear regions in Sy2 galaxies. González Delgado, Heckman & Leitherer (2001) found high-order Balmer lines and He I absorption lines, strong indicators of the presence of YSPs, in their optical spectroscopic study of a sample of 20 Sy2 galaxies. Most of the objects in the González Delgado et al. (2001) sample are classified as LIRGs, and one, Mrk 273, is classified as a ULIRG and included in the work presented here. Therefore, it is straightforward to understand that Comb II, including a power-law, is particularly useful for those

ULIRGs in our sample also classified as Sy2 galaxies at optical wavelengths.

Since the power-law also represents a highly reddened VYSP, Comb II gives an idea of the contribution level of the OSPs in each galaxy. Therefore, we decided to use it for the whole sample of ULIRGs. Adequate fits ($\chi^2 \leq 1.0$) to the overall SED shapes were found for all of the apertures of all objects using this combination. On the other hand, this combination fails to fit the detailed absorption features for 10 per cent (13 apertures) of the apertures modelled. Fig. 5 shows an example of a fit obtained for IRAS 13539+2920 using Comb II for the same extraction aperture shown in Fig. 4. It is clear from the figure that the underprediction of the Ca II K absorption line disappears when a power-law is included. Finally, as shown in Tables 6 and 7 the minimum percentage contribution of the OSP component is less that 10 per cent (due to the uncertainties inherent in the modelling techniques percentage contributions <10 per cent are considered negligible) for most of the apertures. This result suggests that an OSP component is not required to fit the data in the majority of the objects in the ES.

4.3 Combination III

A drawback of Comb II is that, for those cases in which the power-law is likely to represent a VYSP component, it gives no information

Table 8. Modelling results for the CS using Comb III (IYSP + VYSP). Column (1): object name. Column (2): aperture label as indicated in Fig. 2. Column (3): range of ages for the IYSP component that adequately fit the data. Column (4): range of $E(B - V)$ values for the IYSPs in Column (3). Column (5): range of ages of the VYSP that adequately fit the data. Column (6): range of $E(B - V)$ values for the VYSPs in Column (5). Column (7): flux contributions of the VYSP components to the model, in the normalizing bin.

Object name IRAS (1)	Aperture (2)	Age of IYSP (Gyr) (3)	$E(B - V)$ of IYSP (4)	Age of VYSP (Myr) (5)	$E(B - V)$ of VYSP (6)	Per cent VYSP (7)
00091−0738	5 kpc	0.5–1.0	0.0–0.4	6–50	0.5–1.0	30–65
	Ap A	0.7–2.0	0.0–0.2	≤100	0.0–1.5	≤50
	Ap B	0.3–2.0	0.0–0.4	≤100	0.2–1.0	10–90
00188−0856	5 kpc	0.5–0.7	0.0–0.4	≤100	0.2–1.6	≤40
01004−2237	5 kpc	0.5–0.7	0.2–0.4	9–20	0.1–0.3	60–75
12072−0444	5 kpc	0.7–2.0	0.0–0.4	7–20	0.4–0.6	45–65
	Ap A	0.5–2.0	0.0–0.4	≤100	0.0–1.2	20–65
	Ap B	1.0–2.0	0.0	40–100	0.0–0.3	40–60
12112+0305	5 kpc-I	0.5–1.0	0.0–0.4	7–40	0.5–0.8	50–90
	5 kpc-II	0.3–2.0	0.0–0.4	4–60	0.0–0.5	35–90
	Ap A	0.5–2.0	0.0–0.4	≤50	0.6–1.0	35–80
12540+5708	5 kpc	–	–	–	–	–
	Ap A	2	0.0	5–10	0.0–0.1	30–35
	Ap B	0.5–2.0	0.0–0.4	10–100	0.1–0.5	30–65
	Ap C	0.3–2.0	0.0–0.4	50–80	0.0–0.1	70–96
	Ap D	–	–	–	–	–
	Ap E	0.7–2.0	0.0–0.4	6–70	0.5–1.0	40–75
13428+5608	5 kpc	0.7–2.0	0.0–0.4	6–50	0.4–0.8	20–50
	Ap A	0.7–2.0	0.0–0.2	≤100	0.0–0.6	5–50
	Ap B	2.0	0.0	50–100	0.4–0.5	25–33
	Ap C	0.7–2.0	0.0–0.2	≤100	0.0–0.8	10–50
	Ap D	0.7–2.0	0.0–0.4	5–60	0.3–0.8	25–60
	Ap E	0.7–2.0	0.0–0.4	6–50	0.4–0.8	20–50
	Ap F	0.7–2.0	0.0–0.4	5–60	0.3–0.6	25–55
13451+1232 (PA160)	5 kpc	2.0	0.0–0.2	≤100	0.0–2.0	≤10
	Ap A	2.0	0.0–0.1	≤100	0.0–2.0	≤10
	Ap B	2.0	0.1–0.2	≤100	0.0–1.4	5–20
	Ap C	1.0–2.0	0.1–0.2	≤100	0.1–0.8	20–35
	Ap D	1.0–2.0	0.0–0.2	≤100	0.0–0.9	5–15
13451+1232 (PA230)	Ap A	2.0	0.0–0.1	≤100	0.0–2.0	≤12
	Ap B	2.0	0.1	≤100	0.0–2.0	≤11
13539+2920	5 kpc-I	0.5–2.0	0.0–0.2	10–100	0.2–0.5	15–60
	5 kpc-II	0.7–1.0	0.0–0.4	≤50	0.8–1.5	40–70
14060+2919	5 kpc	0.5–0.7	0.4	7	0.4–0.5	60–100
	Ap A	0.5 - 2.0	0.0–0.2	≤100	0.0–0.9	25–55
	Ap B	0.3–0.7	0.0–0.4	7–30	0.1–0.4	45–90
	Ap C	0.3–0.7	0.0–0.4	4–7	0.2–0.4	45–82
14348−1447	5 kpc-I	0.3–0.7	0.0–0.6	5–20	0.4–0.7	50–80
	5 kpc-II	0.3–2.0	0.0–0.4	7–8	0.4–0.6	40
				50–80	0.0–0.3	50–80
	Ap A	0.3–2.0	0.0–0.4	5–60	0.0–0.5	45–100
	Ap B	0.5–1.0	0.0–0.4	≤30	0.5–1.2	35–60
	Ap C	0.3–2.0	0.0–0.4	≤100	0.0–0.9	14–80
	Ap D	0.5–0.7	0.2–0.4	4–50	0.0–0.6	20–80
14394+5332	5 kpc-I	0.5–0.7	0.2	6–7	0.7	75
	5 kpc-II	2.0	0.0–0.2	6–100	0.0–0.8	25–40
	A	0.5–2.0	0.0–0.4	4–100	0.0–0.5	30–75
	B	0.7–2.0	0.0–0.2	7–40	0.3–0.5	30–55
15130+1958	5 kpc	0.3–1.0	0.0–0.4	≤100	0.0–1.3	20–70
15206+3342	5 kpc	0.5–0.7	0.5–0.6	1–3	0.4–0.5	70–80
		0.3–2.0	0.0–0.4	10	0.3	91
15327+2340 (PA160)	5 kpc	0.5–0.7	0.4	≤60	0.8–1.3	16–45
	Ap A	0.6–0.7	0.0–0.2	≤100	0.0–0.2	<5
	Ap B	0.5–0.7	0.0–0.2	≤100	0.0–0.3	<20
	Ap C	0.5–0.7	0.3–0.5	≤100	0.0–1.0	5–15
	Ap D	0.5–0.9	0.0–1.0	≤80	0.9–1.8	30–63

Table 8 – *continued*

Object name IRAS (1)	Aperture (2)	Age of IYSP (Gyr) (3)	$E(B-V)$ of IYSP (4)	Age of VYSP (Myr) (5)	$E(B-V)$ of VYSP (6)	Per cent VYSP (7)
	Ap E	0.5–0.9	0.2–0.6	≤60	0.9–1.6	22–47
	Ap F	0.5–0.7	0.2–0.6	≤80	0.0–1.5	5–36
	Ap G	0.5–0.7	0.0–0.3	≤70	0.0–0.7	5–20
	Ap$_{TOTAL}$	0.5–0.7	0.2–0.6	≤100	0.0–1.5	5–35
15327+2340 (PA75)	Ap A	0.5–0.7	0.2–0.5	≤100	0.0–2.0	<20
	Ap B	0.5–0.7	0.2–0.6	≤100	0.0–1.0	5–25
	Ap C	0.5–0.7	0.2–0.6	≤50	0.0–1.2	5–30
	Ap D	0.5–0.7	0.2–0.6	≤60	0.0–1.5	5–25
	Ap E	0.5–0.7	0.2–0.5	≤50	0.0–2.0	<30
	Ap F	0.6–0.9	0.1–0.4	≤100	0.0–1.2	<25
	Ap G	0.7–0.9	0.0–0.3	≤100	0.0–0.8	<25
	Ap$_{TOTAL}$	0.5–0.7	0.2–0.5	≤100	0.0–1.2	5–25
15327+2340 (PA75*)	Ap A	0.5–0.7	0.0–0.3	≤60	0.0–0.6	10–35
	Ap B	0.5–0.7	0.0–0.3	≤100	0.0–1.5	5–25
	Ap C	0.5–0.7	0.0–0.3	≤100	0.0–1.5	<40
	Ap D	0.5–0.8	0.0–0.3	≤60	0.0–1.5	<40
	Ap E	0.6–0.9	0.0–0.3	≤60	0.0–1.0	<25
	Ap F	0.6–0.9	0.0–0.3	≤100	0.0–2.0	<15
	Ap$_{TOTAL}$	0.5–0.8	0.0–0.3	≤60	0.0–1.5	5–30
16474+3430	5 kpc-I	0.5–0.7	0.0–0.4	7–8	0.3–0.4	65–80
	5 kpc-II	0.5–2.0	0.0–0.2	6–8	0.2–0.4	30–50
				50–90	0.0–0.2	50
	Ap A	0.5–2.0	0.0–0.4	6–8	0.3–0.5	40–75
				30–40	0.3–0.5	40–75
16487+5447 NE	5 kpc	2.0	0.1	≤80	0.0–0.8	10–20
	Ap A	2.0	0.0–0.2	5–8	0.2–0.3	45–55
				30–40	0.0–0.2	50–60
16487+5447 NW	5 kpc	0.5–0.7	0.0–0.4	4–20	0.1–0.3	55–85
	Ap A	0.5–2.0	0.0–0.4	4–60	0.0–0.4	15–65
	Ap B	0.7–2.0	0.0–0.4	4–8	0.2–0.3	65–80
17028+5817 NE	5 kpc	0.5–1.0	0.0–0.4	4–8	0.3–0.5	50–65
17028+5817 NW	5 kpc	0.5–1.0	0.0–0.2	≤60	0.8–1.5	40–70
	Ap A	0.5–2.0	0.0–0.4	≤100	0.0–0.9	30–85
20414−1651	5 kpc	0.5–2.0	0.0–0.4	4–100	0.4–0.8	30–65
21208−0519	5 kpc I	0.5–2.0	0.0–0.4	5–50	0.3–0.5	50–82
	5 kpc II	–	–	–	–	–
	Ap A	2.0	0.0	70–100	0.3–0.4	40–50
	Ap B	0.5–2.0	0.0–0.4	4–8	0.0–0.6	35–70
				30–100	0.0–0.6	35–70
22491−1808	5 kpc	0.3–0.5	0.0–0.4	4–8	0.2–0.4	45–75
	Ap A	0.5–2.0	0.0–0.4	≤100	0.0–0.8	25–57
	Ap B	0.3–0.7	0.0–0.4	4–7	0.3–0.4	60–90
	Ap C	0.3	0.2–0.4	5–6	0.2–0.4	44–60
23233+2817	5 kpc	–	–	–	–	–
	Ap A	–	–	–	–	–
	Ap B	–	–	–	–	–
23234+0946	5 kpc I	0.5–2.0	0.0–0.4	6–30	0.4–0.6	60–82
	5 kpc II	1.0–2.0	0.0–0.2	≤100	0.5–1.5	17–37
	Ap A	0.7	0.0	≤20	0.5–0.8	15–25
23327+2913	5 kpc I	–	–	–	–	–
	5 kpc II	–	–	–	–	–
	Ap A	–	–	–	–	–
	Ap B	–	–	–	–	–

about the detailed properties (age and reddening) of such a component. Therefore, in order to better investigate the detailed properties of the VYSPs in the galaxies, we used Comb III. Adequate fits to both the continuum and the detailed absorption features are obtained for all but nine (∼7 per cent) of the extraction apertures modelled. In the minority of the cases for which no adequate fits could be obtained using Comb III, either an OSP or a power-law component was required in addition to an YSP. Fig. 6 shows an example of a fit obtained using Comb III for the same extraction aperture shown in Figs 4 and 5 in the case of IRAS 13539+2920. The figure clearly demonstrates that Comb III provides the best fit to all of the detailed absorption features.

Table 9. Same as Table 8, but for the 10 additional ULIRGs included in the ES.

Object name IRAS (1)	Aperture (2)	Age of IYSP (Gyr) (3)	$E(B-V)$ of IYSP (4)	Age of VYSP (Myr) (5)	$E(B-V)$ of VYSP (6)	Per cent VYSP (7)
08572+3915	5 kpc	0.5–2.0	0.0–0.4	6–70	0.1–0.6	30–90
	Ap A	0.5–2.0	0.0–0.4	≤100	0.0–1.0	10–50
	Ap B	0.3–2.0	0.0–0.2	≤100	0.0–0.5	10–60
	Ap C	0.3–2.0	0.0–0.4	≤100	0.0–0.7	25–100
10190+1322	5 kpc-I	0.7–2.0	0.0–0.4	≤60	0.7–1.1	30–65
	5 kpc-II	0.7	0.2–0.4	50–100	0.8–1.1	30–55
	Ap A	0.5–0.7	0.0–0.2	≤100	0.0–2.0	≤25
	Ap B	0.5–1.0	0.0–0.4	8–30	0.8–0.9	52–66
10494+4424	5 kpc	0.5	0.0–0.2	5–10	1.1–1.3	30–45
				40–60	0.8–0.9	50–70
	Ap A	–	–	–	–	–
	Ap B	0.3–0.7	0.0–0.4	6–60	0.0–0.6	45–75
13305−1739	5 kpc	0.5–2.0	0.0–0.4	4–7	0.4–0.7	50–80
14252−1550	5 kpc	0.5–2.0	0.0–0.4	≤90	0.5–1.3	35–80
	Ap A	0.5–1.0	0.0–0.4	≤100	0.0–2.0	5–80
16156+0146	5 kpc-I	0.7–2.0	0.0–0.4	9–10	0.5	60–80
	5 kpc-II	0.3–2.0	0.0–0.4	≤100	0.0–0.6	20–70
	Ap A	0.5–2.0	0.0–0.4	≤30	0.0–0.7	15–81
17044+6720	5 kpc	0.3–1.0	0.0–0.4	7–40	0.4–0.6	40–87
	Ap A	0.3–2.0	0.0–0.4	≤100	0.0–0.8	30–85
	Ap B	0.3–2.0	0.0–0.4	4–100	0.1–0.4	40–85
17179+5444	5 kpc	0.7–2.0	0.0–0.4	4–100	0.3–1.1	25–60
23060+0505	5 kpc	–	–	–	–	–
	Ap A	1.0–2.0	0.0	6–7	0.7	50–60
				40–60	0.4–0.5	50–60
	Ap B	0.7–2.0	0.0–0.4	10–50	0.0–0.5	30–75
23389+0303	5 kpc-I	0.7–1.0	0.0–0.4	6–8	0-6 0.8	50–72
	5 kpc-II	0.7–2.0	0.0–0.2	≤100	0.2–0.9	25–60
	Ap A	0.5	0.0	10–20	0.7	~40
	Ap B	0.7–2.0	0.0–0.4	7	0.8	75
	Ap C	0.7–1.0	0.0–0.4	5–60	0.2–0.8	35–60
	Ap D	0.7–2.0	0.0–0.2	4–6	0.6–0.7	40–50
				40–100	0.2–0.4	45–70

At this stage, it is worth re-iterating that there is no reason, a priori, to expect a major contribution to the optical emission from a 12.5-Gyr OSP in ULIRGs. The lack of an OSP is also suggested by the results of Comb II and, to a lesser extent, those of Comb I. Therefore, in the following, we will concentrate on the modelling results for Comb III and use those for Comb I and Comb II as additional information, unless otherwise specified.

5 ESTIMATING MASSES AND BOLOMETRIC LUMINOSITIES

It is also possible to estimate the masses and bolometric luminosities associated with the stellar populations detected at optical wavelengths using the modelling results. For this purpose, we extracted and modelled a large aperture including all the structure visible in the 2D frames (and in the spatial cut in Fig. 2) for each object. Assuming that the stellar population mix remains constant across the entire visible extents of the galaxies, we chose a model from all the adequate fits obtained, selected to be as representative as possible of all the stellar populations in the galaxy. Once the model was selected, we estimated the mass contribution of each of the stellar components in the large aperture. Since the slit does not cover the full extent of each galaxy, we then used the Kim et al.

(2002) total magnitudes of the galaxies in the *R*-band to scale the results and estimate the total masses in each of the stellar components. However, due to the diversity of the stellar populations found, it is sometimes hard to select a particular representative model for some ULIRGs. In such cases, the selection is biased towards models consistent with the results obtained for the nuclear region, since it is likely that most of the MFIR luminosity arises from these regions. The estimated total masses of the YSPs (VYSPs plus IYSPs, results presented in Table 10) fall in the range $0.18 \times 10^{10} \le M_{YSP} \le 50 \times 10^{10}$ M$_\odot$. In the cases where both VYSPs and IYSPs are present, the IYSP is, in most cases, more massive than the VYSP (the exceptions are IRAS 10494+4424, IRAS 14252−15550 and IRAS 17028+5817 W).

To estimate the bolometric luminosities associated with the stellar populations detected in the optical, we assumed the same combination of stellar populations as used for the mass measurements, scaling the unreddened stellar templates using the mass values previously obtained. We then integrated the scaled synthetic spectra over their entire wavelength range. The results are presented in Table 10. We find stellar bolometric luminosities in the range of $0.07 \times 10^{12} < L_{bol} < 2.2 \times 10^{12}$ L$_\odot$. Assuming that most of the starlight is absorbed and then reprocessed by dust, we can compare the estimated bolometric luminosities with the MFIR
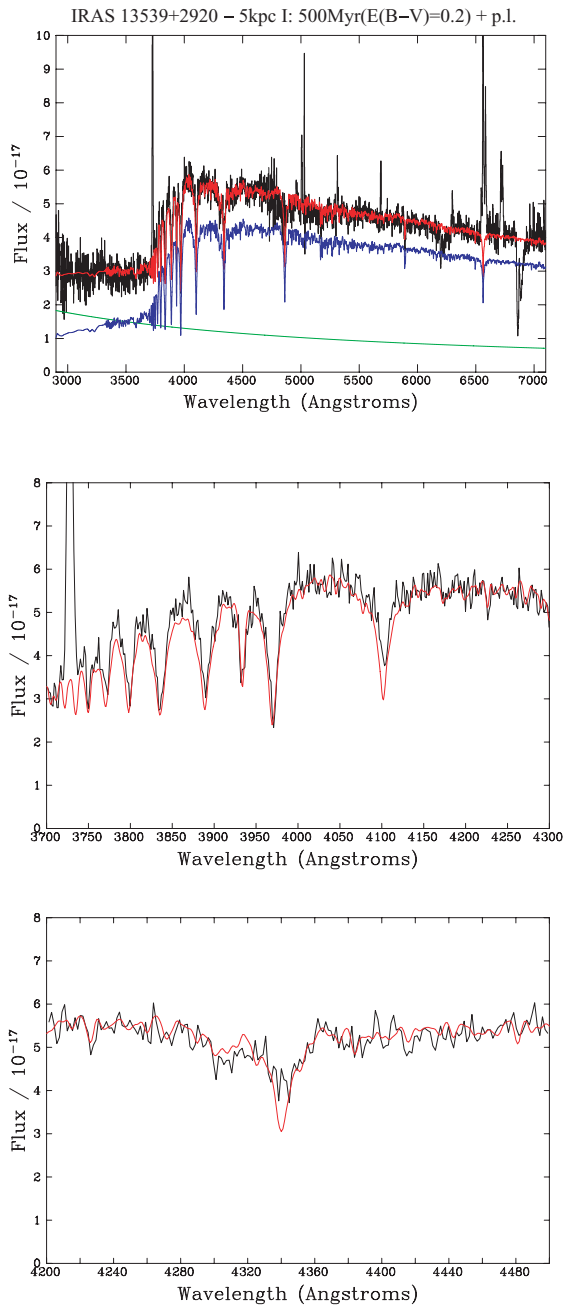
Figure 5. Same as Fig. 4 using Comb II. The figure shows a model comprising a 500-Myr IYSP [$E(B-V) = 0.2$] and a power-law (power-law index $\alpha = -1.06$) which contribute 78 and 21 per cent, respectively, to the flux in the normalizing bin (4600–4700 Å), with no need of a contribution from a 12.5-Gyr OSP. The green, blue and red spectra correspond to the power-law, the IYSP and the sum of the two components, respectively. It is clear from the figure that the underprediction of the Ca II K absorption line disappears when a power-law is included. A small improvement in the fit to the G-band is also present using this combination.

Figure 6. Same as Fig. 4 but using Comb III. The model shown in the figure is composed of 500-Myr IYSP [$E(B-V) = 0.2$] plus a 6-Myr VYSP [$E(B-V) = 0.5$], which contribute 56 and 40 per cent, respectively, to the flux in the normalizing bin (4600–4700 Å). The green, blue and red spectra correspond to the VYSP, the IYSP and the sum of the two components, respectively. In the case of Comb III, both the continuum and the absorption features (high-order Balmer lines, Ca II K and the G-band) are better fitted using this combination than in the case of Comb I and Comb II.

luminosities of the sources, presented in Table 1. Column 7 in the table shows the estimated bolometric luminosities of the YSPs detected in the optical expressed as percentages of the measured MFIR luminosities.

Finally, we emphasize that the results in Table 10 are indicative rather than exact, and they must be interpreted carefully due to the various uncertainties attached to the process. In particular, a major source of uncertainty arises from the selection of the model; different combinations of stellar populations may change the results significantly. Moreover, the fraction of the stellar bolometric luminosity that actually heats the MFIR-radiating dust is uncertain, especially in the extended regions where the reddening is likely to be relatively modest.

Table 10. Estimated total masses and bolometric luminosities associated with the stellar components detected at optical wavelengths. Column (1): object name. Column (2): estimated mass associated with the VYSP component. Column (3): estimated masses associated with the IYSP component. Column (4): estimated masses associated with the OSP component (if present). Column (5): estimated bolometric luminosities associated with the stellar components. Column (6): MFIR luminosity of the sources from Kim & Sanders (1998). Column (7): estimated bolometric luminosities of the YSPs detected in the optical expressed as percentages of the MFIR luminosities.

Object name IRAS	Mass VYSP $(10^9 \, M_\odot)$	Mass IYSP $(10^{10} \, M_\odot)$	Mass OSP $(10^{11} \, M_\odot)$	L_{bol} $(10^{12} \, L_\odot)$	L_{IR} $(10^{12} \, L_\odot)$	Per cent of L_{IR}
(1)	(2)	(3)	(4)	(5)	(6)	(7)
00091−0738	1.8	4.4	–	0.56	1.69	33
00188−0856	7.8	9.3	–	0.24	2.34	10
01004−2237	0.4	1.5	–	0.07	1.90	4
08572+3915	3.9	2.4	–	0.11	1.41	8
10190+1322	3.0	3.6	–	0.83	1.10	75
10494+4424	31.0	2.1	–	0.48	1.48	32
12072−0444	17.4	1.9	–	0.18	2.45	7
12112+0305	0.4	7.2	–	0.21	2.10	10
13305−1739	4.9	3.4	–	1.80	1.78	101
13428+5608	4.3	7.0	–	0.58	1.08	54
13451+1232	4.5	50.0	–	2.10	2.09	100
13539+2920	7.4	2.7	–	0.88	1.10	80
14060+2919	2.1	5.4	–	0.53	1.17	45
14252−1550	46.0	0.7	–	0.96	1.55	62
14348−1447	13.0	9.5	–	0.36	2.09	17
14394+5332E	10.0	1.2	–	0.80	1.20	67
14394+5332W	18.0	2.2	–	0.53	–	–
15130−1958	0.5	4.0	–	0.20	1.23	16
15206+3342	2.2	8.2	–	1.69	1.66	102
15327+2340	0.5	3.5	–	0.16	1.62	10
16156+0146	1.0	3.1	–	0.27	1.20	23
16474+3430	1.1	8.4	–	0.33	1.41	23
16487+5447	3.3	9.0	–	0.17	1.44	12
17028+5817E	1.3	0.5	–	0.22	–	
17028+5817W	41.4	0.9	–	0.65	1.38	47
17044+6720	3.4	2.4	–	0.77	1.48	52
17179+5444	7.5	16.6	–	2.0	1.74	114
20414−1651	0.8	3.4	–	0.32	1.51	21
21208−0519	3.8	9.2	–	0.77	1.12	69
22491−1808	2.7	2.5	–	0.8	1.35	59
23060+0505	19.0	–	0.5	2.2	3.01	73
23233+2817	10.0	–	2.2	0.16	1.1	15
23234+0946	5.2	4.3	–	0.65	1.23	53
23327+2913N	–	–	3.5	–	–	
23327+2913S	1.8	–	1.2	0.23	1.25	18
23389+0303	2.1	1.9	–	0.49	1.35	36

Note that since it was not possible to model the stellar populations in the nuclear regions of the three ULIRGs classified as Sy1 galaxies (IRAS 12540+5708, IRAS 15462−0450 and IRAS 21219−1757), no results for these objects are presented in the table (see Appendix A for details).

6 SUMMARY OF GENERAL PATTERNS AND RESULTS

In order to give an overview of the properties of the stellar populations of the ULIRGs in our sample as a whole, the general results and patterns obtained from the modelling can be summarized as follows.

(i) *Modelling technique.* Three different combinations of stellar populations have been used for the analysis presented here: *Comb I* (OSP + YSP), *Comb II* (OSP + YSP + power-law) and *Comb III* (VYSP + IYSP). In general, adequate fits to the overall shapes of the continua in individual apertures are obtained using all of the combinations. However, Comb I fails to fit the detailed absorption features for 42 per cent (54) of the extraction apertures. This percentage is reduced down to 10 per cent (13 apertures) and 7 per cent (nine

apertures) in the cases of Comb II and Comb III, respectively. Note that adequate fits for both the continuum and the detailed absorption features are found for 60 per cent of the extraction apertures using *all* of the combinations. This clearly demonstrates the difficulty in obtaining a unique solution when using combinations of different stellar populations to model the optical spectra of starburst systems.

(ii) *YSPs.* YSPs ($t_{YSP} \leq 2.0$ Gyr) are present in *all* apertures in *all* sources, with the exception of IRAS 23327+2913 5 kpc-II. Furthermore, VYSPs ($t_{VYSP} \leq 100$ Myr) are essential to obtain adequate fits in *all but* 20 ($\sim$15 per cent) of the extraction apertures, 14 of which sample the extended regions of Arp 220 and the radio galaxy IRAS 13451+1232 (PKS 1345+12).

At this stage we add a caveat about the properties of the so-called IYSPs ($0.1 < t_{IYSP} \leq 2.0$ Gyr). For this component, we have assumed a limited range of ages and, in particular, reddening values,

in comparison with those of the VYSPs. Therefore, the ranges of age and reddening presented in Tables 8 and 9 for the IYSPs are partially a consequence of these assumptions.

(iii) *OSPs.* OSPs (12.5 Gyr) do not make a major contribution to the optical light in most apertures for most sources. The modelling results show that OSPs are essential for fitting the optical continuum in only seven ($\sim$5 per cent) of all the apertures considered; in the majority of the cases, adequate fits can be obtained using combinations of IYSPs and VYSPs. Only in the cases of IRAS 23327+2913 (5 kpc-II) and IRAS 21208−0519 (5 kpc-II) do we find that the OSPs dominate. In addition, in the cases of IRAS 13451+1232, IRAS 14394+5332 5 kpc-II, IRAS 16487+5447E and IRAS 23234+0946 5 kpc-II either OSPs or dominant 'old' IYSPs (1–2 Gyr) are required to model the data.

(iv) *Reddening.* The study presented here further emphasizes the importance of carefully accounting for dust reddening effects when modelling the stellar populations of star-forming galaxies.

(v) *Double nucleus systems.* 20 of the 36 ULIRGs in our sample are classified as double nucleus systems and one, IRAS 14394+5322, is classified as a multiple (>two nucleus) system. For 14 of these systems, it was possible to study the stellar populations within the different nuclei individually. In 71 per cent of the cases (10 of the 14 objects) the results are consistent with the stellar populations being similar in the two nuclei in terms of ages, reddenings and percentage contributions. However, in four cases (IRAS 14394+5332, IRAS 16487+5447, IRAS 21208−0519 and IRAS 23327+2913) we find marked differences between the mix of ages of the stellar populations in the two nuclei.

(vi) *Extended and nuclear apertures.* In the majority of the objects we find that we require the same stellar components (IYSP and VYSP) at all locations of the systems to model the spectra adequately.

(vii) *Masses of the YSP.* The estimated total masses of the YSPs (VYSPs plus IYSPs) fall in the range $0.18 \times 10^{10} \leq M_{YSP} \leq 50 \times 10^{10} \, M_\odot$. In the cases where both VYSPs and IYSPs are present, the IYSP is, in most cases, more massive than the VYSP (the exceptions are IRAS 10494+4424, IRAS 14252−15550 and IRAS 17028+5817 W).

(viii) *Bolometric luminosities.* We have also estimated the bolometric luminosities associated with these stellar populations. For 48 per cent of the objects in the ES sample (16 of the 33 objects, excluding the Sy1 galaxies), the bolometric luminosities of the YSPs detected in the optical represents a large fraction ($\gtrsim$50 per cent) of the MFIR luminosities of the sources.

More detailed information about individual sources is presented in Appendix A.

7 CONCLUSIONS

This is the first of two papers presenting a detailed study of the stellar populations in a large sample of ULIRGs, based on long-slit optical spectroscopic observations. In this paper we have introduced the sample and described the analysis techniques and the general results obtained from the modelling. In addition, we have presented estimated values for the total masses of the stellar populations within the objects and the bolometric luminosities associated with them.

Overall, the results for the sample in general are consistent with those obtained in the detailed studies of RZ07 and RZ08 for PKS 1345+12 and Arp 220, respectively, in terms of

(i) the requirement for a mixture of VYSPs and IYSPs, with the proportional contribution of the VYSP component increasing towards the nuclei in most cases; and

(ii) the importance of taking into account the reddening of the YSP component, with clear evidence of increasing reddening towards the nuclei in a number of the objects.

The work presented here clearly shows the utility of spectral synthesis modelling techniques for studying the properties of the stellar populations in star-forming galaxies. In addition, it also shows the difficulty in obtaining a unique solution when using combinations of different stellar populations to model spectra, especially on the basis of fits to the SED alone (i.e. not examining the detailed absorption features). We have shown that some results, and therefore the conclusions based on them, can change significantly if different models are used.

The results described in this paper will be analysed in more detail in a forthcoming paper (Rodríguez Zaurín et al., in preparation), where they will be discussed in the context of evolutionary models for merging systems, and the results obtained for similar systems in the high-redshift universe.

REFERENCES

Armus L., Heckman T., Miley G., 1990, ApJ, 364, 471
Armus L. et al., 2007, ApJ, 656, 148
Arribas S., Colina L., 2002, ApJ, 573, 576
Arribas S., Colina L., Borne K., 2000, ApJ, 542, 228
Barnes J. E., Hernquist L., 1996, ApJ, 471, 115
Bruzual G., Charlot S., 2003, MNRAS, 344, 1000
Calzetti D., Armus L., Bohlin R., Kinney A., Koornneef J., Storchi-Bergman T., 2000, ApJ, 533, 682
Canalizo G., Stockton A., 2000a, ApJ, 528, 201
Canalizo G., Stockton A., 2000b, AJ, 120, 1750
Canalizo G., Stockton A., 2001, ApJ, 555, 719
Cole G., Pedlar A., Holloway A., Mundell C., 1999, MNRAS, 310, 1033
Condon J., Huang Z.-P., Yin Q., Thuan T., 1991, ApJ, 378, 65
Dasyra K. et al., 2006a, ApJ, 638, 745
Dasyra K. et al., 2006b, ApJ, 651, 835
Davies R., Tacconi L., Genzel R., 2004, ApJ, 613, 781
Dickson R., Tadhunter C. N., Shaw M., Clark N., Morganti R., 1995, MNRAS, 273, L29
Downes D., Solomon P., 1998, ApJ, 507, 615
Evans A., Kim D., Mazzarella J., Scoville N., Sanders D., 1999, ApJ, 521, L107
Evans A., Mazzarella J., Surace J., Sanders D., 2002, AJ, 580, 749
Farrah D., Afonso J., Efstathiou A., Rowan-Robinson M., Fox M., Clements D., 2003, MNRAS, 343, 585
Farrah D., Surace J. A., Veilleux S., Sanders D. B., Vacca W. D., 2005, ApJ, 626, 70
Farrah D. et al., 2007, ApJ, 667, 149
Franceschini A., Aussel H., Cesarsky C. J., Elbaz D., Fadda D., 2001, A&A, 378, 1

Franceschini A. et al., 2003, MNRAS, 343, 1181

Genzel R. et al., 1998, ApJ, 498, 579

González Delgado R., Heckman T., Leitherer C., 2001, ApJ, 546, 845

González Delgado R. M., Cerviño M., Martins L. P., Leitherer C., Hauschildt P. H., 2005, MNRAS, 357, 945

Hamilton D., Keel W., 1987, ApJ, 321, 211

Holt J. et al., 2003, MNRAS, 342, 227

Houck J. et al., 1984, ApJ, 278, L63

Houck J., Sneider D., Danielson G., Beichman C., Lonsdale C., Neugebauer C., Soifer B. T., 1985, ApJ, 290, L5

Imanishi M., Dudley C., 2002, ApJ, 545, 701

Imanishi M., Dudley C., Maloney P., 2006, AJ, 637, 114

Imanishi M., Dudley C., Maiolino R., Maloney P., Nakagawa T., Risaliti G., 2007, ApJ, 171, 72

Kim D. C., Sanders D. B., 1998, ApJ, 119, 41

Kim D. C., Veilluex S., Sanders D. B., 2002, ApJ, 143, 277

Kim D. C. et al., 1998, ApJ, 508, 627

Knapen J., Laine S., Yates J. A., Robinson A., Richards A., Doyon R., Nadeau D., 1997, ApJ, 490, L29

Leitherer C. et al., 1999, ApJ, 123, 3

Lutz D., Veilluex S., Genzel R., 1999, ApJ, 517, L13

Majewski S., Hereld M., Koo D., Illingworth G., Heckman T., 1993, ApJ, 403, 125

Mihos J. C., Hernquist L., 1996, ApJ, 464, 641

Murphy T., Soifer B., Matthews K., Armus L., 2001, ApJ, 559, 201

Nagar N., Wilson A., Falcke H., Veilleux S., Maiolino R., 2003, A&A, 409, 115

Osterbrock D., Fulbright J., Keane M., Trager S., 1996, PASP, 108, 277

Rigopoulou D., Spoon H., Genzel R., Lutz D., Moorwood A., Tran Q., 1999, ApJ, 118, 2625

Risaliti G. et al., 2006, MNRAS, 365, 303

Robinson T., Tadhunter C., Axon D., Robinson A., 2000, MNRAS, 317, 922

Rodríguez Zaurín J., Holt J., Tadhunter C., González Delgado R., 2007, MNRAS, 375, 1133 (RZ07)

Rodríguez Zaurín J., Tadhunter C. N., González Delgado R. M., 2008, MNRAS, 384, 875 (RZ08)

Rupke D., Veilleux S., Sanders D., 2002, ApJ, 570, 588

Rupke D. S. et al., 2005, ApJ, 632, 751

Salpeter E., 1955, ApJ, 121, 161

Schlegel J., Finkbeiner D., Davis M., 1998, ApJ, 500, 525

Scoville N. Z. et al., 2000, ApJ, 119, 991

Seaton M., 1979, MNRAS, 187, 73

Soifer B. et al., 1984a, ApJ, 278, L71

Soifer B. et al., 1984b, ApJ, 283, L1

Soifer B., Sanders D., Neugebauer C., Danielson G., Lonsdale C., Madore B., Persson S., 1986, ApJ, 303, L41

Soifer B., Sanders D., Madore B., Neugebauer C., Danielson G., Elias E., Lonsdale C., Rice W., 1987, ApJ, 320, 74

Soifer B. et al., 2000, AJ, 119, 509

Springel V. et al., 2005, MNRAS, 361, 776

Surace J. A., Sanders D. C., 1999, ApJ, 512, 162

Surace J. A., Sanders D., 2000, ApJ, 120, 604

Surace J. A., Sanders D. B., Vacca W. D., Veilleux S., Mazzarella J. M., 1998, ApJ, 492, 116

Surace J., Sanders D., Evans A., 2000, ApJ, 529, 170

Tadhunter C., Dickson R., Morganti R., Robinson T., Wills K., Villar-Martin M., Hughes M., 2002, MNRAS, 330, 977

Tadhunter C. N., Robinson T. G., González Delgado R. M., Wills K., Morganti R., 2005, MNRAS, 356, 480

Ulvestad J. S., Wilson A., 1984, ApJ, 278, 544

Valdés J., Berta S., Bressan A., Franceschini A., Rigopoulou D., Rodighiero G., 2005, A&A, 434, 149

Veilleux S., Kim D. C., Mazzarella J. M., Soifer B. T., 1995, ApJ, 98, 171

Veilleux S., Sanders D., Kim D.-C., 1997, ApJ, 484, 92

Veilleux S., Kim D.-C., Sanders D. B., 1999a, ApJ, 522, 113

Veilleux S., Sanders D. B., Kim D.-C., 1999b, ApJ, 522, 139

Veilleux S., Kim D. C., Sanders D. B., 2002, ApJ, 143, 315

Veilluex S. et al., 2006, ApJ, 643, 707

Wilson C., Harris W., Longden R., Scoville N., 2006, ApJ, 641, 763

APPENDIX A: NOTES ON INDIVIDUAL SOURCES

IRAS 00091−0738. Optical and near-IR images reveal the presence of several bright knots showing the location of young ($\lesssim$7 Myr) stellar populations (Surace et al. 2000) in this double nucleus system (nuclear separation, NS = 2.2 kpc). The double nucleus structure is not resolved in our spectra and a single 5-kpc aperture was used during the analysis. Our modelling results reveal the presence of a significant contribution from VYSPs in the nuclear region, which is consistent with the results obtained for the extended apertures. IRAS 00091−0738 is classified as an H II galaxy at optical wavelengths. Therefore, it is possible to use the nebular emission lines in order to provide a further constraint on the ages of the VYSP component. The VYSP age obtained using the Hα equivalent width and the Leitherer et al. (1999) models [EW(Hα) = 28 Å, t_{VYSP} ∼ 7 Myr] is consistent with the lower end of the range of ages found from the modelling.

IRAS 00188−0856. This compact, single nucleus system is classified as a LINER at optical wavelengths. On the other hand, Valdés et al. (2005) and Imanishi et al. (2007) reported evidence of the presence of an AGN in the nucleus of the galaxy based on their near- and mid-IR studies of the object. However, the AGN does not dominate the IR emission, which is likely to be dominated by starburst activity (Lutz et al. 1999; Valdés et al. 2005). The modelling results suggest the presence of a dominant IYSP with a relatively small percentage contribution of any VYSP. Note that, due to the small contribution of the VYSP to the optical light from the galaxy, both the age and reddening of that component are relatively unconstrained.

IRAS 01004−2237. The optical spectrum of this single nucleus system shows a mixture of H II and Sy2 features (Veilleux et al. 1999a), with clear evidence of a buried AGN at IR wavelengths (Imanishi et al. 2007). The modelling results clearly suggest the presence of a dominant VYSP with relatively low reddening. The VYSP ages obtained from the modelling (t_{VYSP} = 9–20 Myr) differ from those obtained from the Hα equivalent width [EW(Hα) = 58 Å, t_{VYSP} ∼ 6.5 Myr]. However, given the uncertainties attached to the synthetic templates for very young ages ($\leq$10 Myr), we consider that ∼3 Myr is not a major disagreement between the two results.

IRAS 08572+3915. This is double nucleus system consisting of two spirals galaxies in the process of merging, rotating in different planes (Arribas, Colina & Borne 2000). The nuclear, 5-kpc aperture was centred in the northern nucleus (the secondary nucleus was not covered by the slit), thought to be responsible for the far-IR emission from the source (Condon et al. 1991; Soifer et al. 2000; Evans et al. 2002; Nagar et al. 2003). The *Hubble Space Telescope* (*HST*)-Wide-Field Planetary Camera 2 (WFPC2) image taken by Surace et al. (1998) reveals the presence of several young (t_{knots} = 5–10 Myr), massive knots located in both the tails and the nuclear regions. The optical spectrum of IRAS 08572+3915 is a composite of H II and LINER-like features. Although no evidence for the presence of an AGN is found in the optical and near-IR (Veilleux, Kim & Sanders 1999a; Veilleux, Sanders & Kim 1999b), IRAS 08572+3915 shows signs of AGN activity at mid-IR wavelengths (Imanishi & Dudley 2002; Imanishi, Dudley & Maloney 2006; Armus et al. 2007). Moderately reddened VYSPs are found in the northern nucleus, which contribute significantly to the optical light. The reddenings and ages

of the stellar components in the extended apertures are consistent with those of the nuclear aperture.

IRAS 10190+1322. The north-east galaxy of this double nucleus system is brighter at near-IR and radio wavelengths (Murphy et al. 2001; Nagar et al. 2003; Dasyra et al. 2006b), while the south-western nucleus appears the brightest in the optical. Recently, Rupke, Veilleux & Sanders (2002) classified the north-east nucleus as a LINER and the south-western source as an H II galaxy in their high-resolution spectroscopic study of ULIRGs. No evidence for AGN activity is found at near- and mid-IR wavelengths (Veilleux et al. 1999b; Imanishi et al. 2007), which is consistent with the idea of starburst activity powering the IR luminosity of the source (Farrah et al. 2003). The results obtained from the modelling suggest that the VYSPs are concentrated in the two nuclei of the galaxy, and in the region in between, coinciding with large concentrations of gas and dust. In this case, only the extracted spectrum from aperture 5 kpc-I shows clear H II-like region features. The VYSP age derived using the Hα equivalent width [EW(Hα) = 47 Å, $t_{VYSP} \sim 6.5$ Myr] for that region of the galaxy is consistent with the lower end of the range of ages found for the VYSPs from modelling the optical continuum.

IRAS 10494+4424. The modelling results obtained using near-IR and optical photometric points clearly suggest a starburst as an ionizing source for this single nucleus system (Farrah et al. 2003), which is classified as a LINER in the optical (Kim & Sanders 1998). Modelling the optical spectra, we find that the VYSPs located in the nuclear and the northern region of the galaxy make a significant contribution to the optical light. However, adequate fits for Ap A (sampling a region towards the south of the galaxy) are only obtained using Comb I, with the optical light dominated by a 400-Myr IYSP with little or no reddening, plus a small contribution from a 12.5-Gyr OSP. In terms of reddening, our modelling results clearly provide evidence for higher reddenings towards the nuclear regions of the galaxy.

IRAS 12072−0444. This ULIRG appears as a single nucleus system in the optical and near-IR images of Kim et al. (2002). However, a second nucleus becomes apparent in the *HST*-NICMOS (Near Infrared Camera and Multi-Object Spectrometer) *H*-band images (Veilluex et al. 2006). This second nucleus was first detected in the WFPC2 images of Surace et al. (1998), but was classified as a super star cluster. More recently, Dasyra et al. (2006a) confirmed spectroscopically the presence of a second genuine nucleus, with a NS = 2.8 kpc. The double nucleus structure is unresolved in our spectroscopic data. The detection of strong [Si IV] emission is evidence for the presence of a buried AGN in this source, classified as a Sy2 galaxy in the optical (Veilleux et al. 1995; Kim & Sanders 1998). Moderately reddened VYSPs which contribute significantly to the optical light from the galaxy are located in the nuclear region. Comparing the nuclear with the extended apertures, the modelling results suggest the presence of younger, more highly reddened VYSPs in the nuclear regions of the galaxy than in the extended apertures.

IRAS 12112+0305. This double nucleus system is classified as a LINER in the optical, shows no evidence for powerful AGN activity (Genzel et al. 1998; Veilleux et al. 1999b), and is classified as a star-burst at all other wavelengths studied (Lutz et al. 1999; Franceschini et al. 2003; Risaliti et al. 2006; Armus et al. 2007). The modelling results show the presence of dominant, relatively high reddened VYSPs located in the north-eastern nucleus (5 kpc-I), which is the
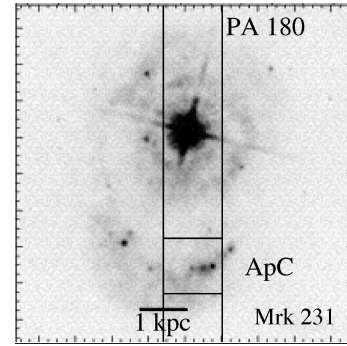

Figure A1. Mrk 231: the slit position and the location of Ap C are shown in the figure superimposed on the Surace et al. (1998) F439W WFPC2 *HST* image. The major ticks are arcseconds.

brightest at optical wavelengths. For this object, the ages and per-centage contributions to the flux for both nuclei and the region in between are consistent. On the other hand, our results suggest increasing concentrations of obscuring dust towards the northern source.

IRAS 12540+5708. Also known as Mrk 231, IRAS 12540+5708 is the most luminous ULIRG in our sample [log(L_{IR}) = 12.54]. This object is classified as a Sy1 galaxy in the optical, and considered an AGN-powered ULIRG based on mid- and near-IR spectroscopy (Lutz et al. 1999; Rigopoulou et al. 1999). However, the fraction of the bolometric luminosity produced by the AGN remains contro-versial. Despite its warm MFIR colours, Davies, Tacconi & Genzel (2004) found that star formation within the inner 300 pc is respon-sible for 25–40 per cent of the entire luminosity of the galaxy, and that starburst activity seems to power most of the far-IR luminosity (Downes & Solomon 1998; Farrah et al. 2003). On the other hand, ages from a few Myr in the inner parts of the galaxy, up to ages of order of Gyr in the extended regions, have been found for the stellar populations in the galaxy (Surace et al. 1998; Canalizo & Stockton 2000a; Davies et al. 2004).

Because of ghost images affecting many of the apertures in the red arm, it was only possible to model the extracted spectra from the blue arm, with the exception of Ap C. In addition, the powerful AGN emission prevents any attempt at modelling the stellar populations for those apertures sampling the nuclear regions (5 kpc and Ap D). Therefore, only the extracted spectra from apertures A, B, C and E were used for the analysis of the stellar populations presented here. Note that Ap C samples the bright condensation (the 'horseshoe'; Hamilton & Keel 1987) ~3 kpc to the south of the galaxy, as seen in the *HST*-WFPC2 images taken by Surace et al. (1998). Fig. A1 shows the position of the slit and the extent of Ap C, superimposed on the Surace et al. (1998) *HST*-WFPC2 F439W image. In order to minimize the potential AGN contamination (including the seeing disc of the bright AGN and any dust-scattered AGN light), the spatial axes of the blue and red 2D frame were reversed. The reversed and the original frames were registered and then subtracted. A spatial cut of the subtracted 2D frame is shown in Fig. A2, as well as the spatial cut of the original frame and the extent of Ap C. It is clear from the figure that any AGN contamination has been removed, and therefore, we were able to model the full spectral range for this aperture.

The modelling results for Ap C reveal the presence of a VYSP with a low reddening [$E(B − V) = 0.0$–0.1] and ages in the range $50 \le t_{VYSP} \le 80$ Myr, that accounts for almost the entire optical light
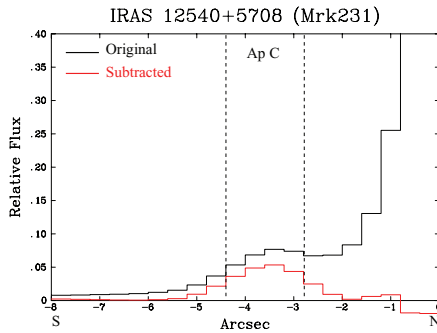
Figure A2. Mrk 231: spatial cuts (4400–4600 Å) extracted from the subtracted and original 2D frames showing the region including the bright condensation to the south of the galaxy. It is clear from the figure that the AGN contamination has been almost entirely removed after applying the technique described in the text. The location of Ap C is also shown in the figure.
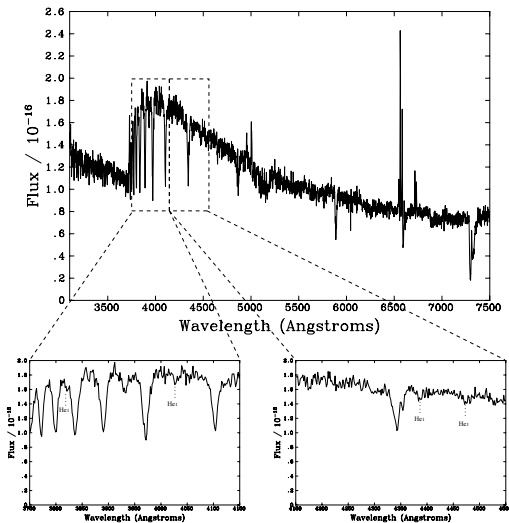

Figure A3. Extracted spectrum from Ap C for Mrk 231. The figure shows the detection of the He I absorption lines at 3820, 4026, 4388 and 4471 Å. These lines have a maximum strength for ages in the range of 20–50 Myr, and are not produced by stellar populations older than 100 Myr.

within the aperture (P_{VYSP} = 70–96 per cent). It is worth noting that Comb I, Comb II and Comb III provide consistent results for this aperture. In addition, the extracted spectrum shows the clear presence of He I absorption features at various wavelengths, which are indicated in Fig. A3. In the models, the He I lines are strongest for single stellar populations (SSP) with ages in the range 20–50 Myr, when the stellar population is dominated by B stars (González Delgado et al. 2005), and are not observed in stellar populations older than 100 Myr (the lifetime of B stars). Therefore, the presence of such features helps to provide a further constraint on the age of the VYSP component within the aperture. The detection of the He I absorption lines is consistent with the lower end of the range of ages of the VYSP component deduced from modelling the continuum.

Previous spectroscopic studies already revealed the presence of YSPs in the host galaxy of Mrk 231 (Hamilton & Keel 1987; Canalizo & Stockton 2000b). Canalizo & Stockton (2000b) car-

ried out a similar study to that presented here, modelling the optical spectra extracted from a series of apertures sampling various regions of the galaxy. In order to fit the extracted spectra, they used a combination of a 10-Gyr OSP plus unreddened YSPs with varying ages. This is similar to the Comb I used here, although reddening effects are only fully considered in this study. Their 'regions' a, b, c and k are similar to our Ap C, Ap B, Ap A and Ap E, respectively, shown in Fig. 2. They found YSPs with ages of 5, 140^{+80}_{-70} and 42^{+22}_{-17} Myr for region c, b and a, respectively, which is consistent with the modelling results found here using Comb I. On the other hand, they found no evidence for significant YSPs in region k, similar to the Ap E used here. However, we find important YSPs (YSP per cent = 50–70 per cent) within that aperture, with ages and reddening in the range of t_{YSP} = 60–100 Myr and $E(B - V)$ = 0.2–0.5. This difference is likely to be due to the fact that the rest wavelength range of the spectra used in their study is 3800–7000 Å. Therefore, they do not sample the near-UV, which is a crucial region of the spectrum for constraining the properties of the YSPs. In addition, it is notable that only unreddened synthetic templates are used in the Canalizo & Stockton (2000b) study, whilst reddened YSPs are required to fit the data in the case of Ap E.

IRAS 13305−1739. The optical spectrum of this very compact ULIRG is that of a Sy2 galaxy. In addition, Veilleux et al. (1999b) found broad Paα and [Si IV] emission at near-IR wavelengths – clear evidence of the presence of a quasar/AGN – in the nucleus of the galaxy. A single nuclear aperture was used for the analysis of the stellar populations in this object. We find a moderately reddened, dominant VYSP component with a remarkably narrow range of ages ($4 \leq t_{VYSP} \leq 7$ Myr).

IRAS 13428+5608. Also known as Mrk 273, this galaxy shows an impressive tidal tail extended over 30 kpc towards the south of the galaxy. Seen as a single-nucleus object in UV/optical images (Surace et al. 2000; Kim et al. 2002), a double nucleus structure emerges at near-IR (Armus, Heckman & Miley 1990; Majewski et al. 1993; Knapen et al. 1997; Scoville et al. 2000) and radio (Ulvestad & Wilson 1984; Condon et al. 1991; Cole et al. 1999) wavelengths, with a nuclear separation of ∼700 pc. The double nucleus structure is unresolved in our spectroscopic data. Classified as a Sy2 at optical wavelengths, IRAS 13428+5608 is a composite object powered by both starburst and AGN activity (Armus et al. 2007). However, the dominant power source remains controversial.

In order to perform a detailed study of the stellar populations detected at optical wavelengths, a total of seven apertures were extracted, sampling the nuclear region and the large tidal tail. In the case of the nuclear 5-kpc aperture, we find an 'old' IYSPs (t_{IYSP} = 0.7–2.0 Gyr) with low reddening which dominates the optical emission, with a smaller contribution from a VYSP component with higher reddening. Previous optical spectroscopy already revealed the presence of a mix of stellar populations in the nuclear region of Mrk 273 (González Delgado et al. 2001). In a broad-brush sense, the results presented here are consistent with those of González Delgado et al. (2001). The extended apertures sample the prodigious tidal tail to the south of the galaxy and the north of the nuclear region. Overall, the results show a remarkable uniformity, with a dominant 'old' IYSP present at all locations in the galaxy, out to a radius of 30 kpc. It is also notable that a VYSP component is required in order to fit the data for all the apertures, even for those sampling the extended tail. No evidence suggesting the presence of important age or reddening variations across the body of the galaxy is found in the case of Mrk 273.

IRAS 13451+1232. Also known as PKS 1345+12, this is the only ULIRG in our sample also classified as a radio galaxy. The activity is concentrated in the western nucleus, which is the only nucleus covered by the two slit positions used for this object. This nucleus is classified as a Sy2 in the optical (Veilleux et al. 1999a), and a compact source at radio wavelengths (Evans et al. 1999). Significant YSPs have already been detected in PKS 1345+12 at optical and near-IR wavelengths (Surace et al. 1998; Tadhunter et al. 2005), which may have been formed as a consequence of the merger.

A detailed analysis of the stellar populations within the galaxy, using the so-called Comb I, was already presented for this object in RZ07. We emphasize that prior to modelling the data for both the RZ07 study and this work, we subtracted the best model for the nebular continuum emission from the detailed emission line modelling work of Holt et al. (2003), in the case of the 5-kpc aperture (i.e. the 'NUC' aperture in RZ07). Such emission is also likely to be important in the cases of Ap A and Ap B in PKS 1345+12. For these two apertures, both the results from the modelling using the nebular corrected and uncorrected spectra are presented in Table 4.

In this study, we use an updated version of the code that allows a more detailed analysis of the different, important regions of the optical spectra and, therefore, it is possible to refine the results presented in RZ07. In addition, the extracted spectra are also modelled using Comb II and Comb III. In general terms, the results found here are consistent with those of RZ07, suggesting that a VYSP may not be as important in the case of PKS 1345+12 as for other ULIRGs. In addition, we find that adequate fits are also obtained for all the apertures with an 'old' IYSPs ($t_{IYSP} = 1.0$–2.0 Gyr) that dominate the flux at all locations sampled by the apertures. Because of the small percentage contribution of the VYSP component, the age and reddening of this component are relatively unconstrained, which explains the wide range of ages and reddening presented in Table 8. Finally, note that this is the most massive galaxy in our sample, in terms of its stellar population.

IRAS 13539+2920. Two 5-kpc apertures, sampling the two nuclei of this double nucleus system, were extracted for this object. For the western nucleus (5 kpc-II), which is the brightest at optical wavelengths, we find highly reddened VYSPs that contribute significantly or dominate the optical emission. For the eastern nucleus (5 kpc-I), we find ages consistent with those of the western source, but with lower reddening values. On the other hand, IRAS 13539+2920 is spectroscopically classified as an H II galaxy in the optical. However, modelling the emission lines of the extracted spectra for aperture 5 kpc-II, sampling the nucleus to the west of the galaxy, we find [O III] 5007/Hβ and [N II]6583/Hα emission-line ratios consistent with a combination of an H II galaxy and a LINER. Moreover, the 1D spectrum of that nucleus shows clear signs of line splitting, indicating the presence of ionized gas outflows. On the other hand, no evidence of H II-like region features is found in the case of the eastern source, sampled by aperture 5 kpc-I (it has a LINER spectrum). Therefore, no attempt to estimate the age of the VYSP using the Hα equivalent width was made for this galaxy.

IRAS 14060+2919. We find a moderately reddened, 7-Myr VYSP component that dominates the optical emission in the nuclear region of this single nucleus system. In general terms, the results for the extended apertures are consistent with those in the nuclear region, except for perhaps a slightly smaller VYSP contribution in Ap A (although Ap A is not so well constrained because it is noisier). In addition, IRAS 14060+2919 is classified as an H II galaxy at optical

wavelengths. The Hα equivalent widths measured for Ap B, Ap C and 5 kpc [$77 \leq$ EW (Hα) ≤ 177 Å] reveal the presence of VYSPs younger than $\sim$6 Myr, which is consistent with the continuum modelling results.

IRAS 14252−1550. Classified as a LINER in the optical, no signatures of buried quasar activity are found in the 5-35 μm mid-IR spectrum of this double nucleus system (Imanishi et al. 2007). The modelling results are consistent with a wide range of VYSPs ages, reddenings and percentage contributions. No clear evidence suggesting the presence of important age or reddening variations is found.

IRAS 14348−1447. This is a double nucleus system, in which the ULIRG activity is likely associated with the southern nucleus, which dominates the near-IR luminosity. Several bright knots are seen in the in the U'-, B- and I-band images (Surace et al. 2000; Surace & Sanders 2000), some of the knots with estimated ages younger than 5–7 Myr (Surace et al. 2000). The optical spectrum of IRAS 14348−1447 is that of a LINER (Veilleux et al. 1995; Kim & Sanders 1998), and is classified as starburst-powered ULIRG at near-IR, mid-IR and X-ray wavelengths (Veilleux, Sanders & Kim 1997; Genzel et al. 1998; Lutz, Veilluex & Genzel 1999; Farrah et al. 2003; Franceschini et al. 2003; Risaliti et al. 2006). We find significant, or even dominant VYSPs, with a wide range of reddening values, located in the nuclei of the system. Note that in the case of the north-eastern nucleus (5 kpc-II) the model solutions for the VYSPs divide into two groups: a younger group of 7–8 Myr, and a second, older, group with ages of 50–80 Myr. In this case, we cannot distinguish between the two groups using the detailed fits. However, modelling the emission lines of the extracted spectra for aperture 5 kpc-II we find [O III]5007/Hβ and [N II]6583/Hα emission-line ratios consistent with an H II galaxy. The VYSP age obtained using the Hα equivalent width [EW(Hα) = 51 Å, $t_{VYSP} \sim$ 6.5 Myr] is consistent with the first group of adequate fits, including the younger YSP component. Finally, no evidence is found for significant variations in the YSP age and reddening across the body of the galaxy.

IRAS 14394−1447. This IRAS source is a multiple ($>$two nucleus) system, with the two main components separated by 54 kpc – the widest nuclear separation in the ES. The eastern nucleus is classified as a Sy2 and identified with the source responsible for the far-IR luminosity (Veilleux et al. 1999a; Rupke et al. 2005). Dominant, highly reddened VYSPs are found for that nucleus (5 kpc-I). On the other hand, the modelling results are consistent with a wide range of age and reddening for the VYSP component in the case of the 5-kpc aperture extracted for the western source (5 kpc-II). Moreover, adequate fits are only obtained for that aperture using a 2-Gyr IYSP which, in fact, dominates the flux contribution in the normalizing bin. These results clearly demonstrate large differences between the stellar populations in the two nuclei, perhaps indicating the presence of a more powerful starburst activity in the eastern component. In addition, two further apertures were extracted to the east and west of the western source. We find no clear evidence for the presence of large age and/or reddening variations across the body of that source.

IRAS 15130−1958. The modelling results are consistent with VYSPs with a wide range of ages, reddenings and percentage contributions for the single 5-kpc aperture extracted for this single nucleus system, classified as a Sy2 in the optical. In addition, Wolf–Rayet (WR) features are detected for this galaxy. The detection of such features indicates ongoing star formation activity. Fig. A4
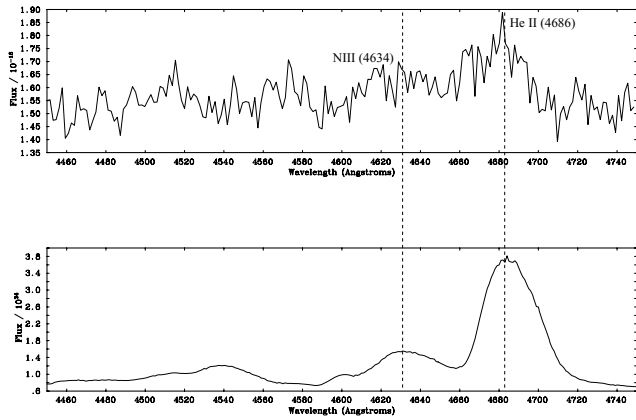
Figure A4. Comparison between the spectrum of IRAS 15130−1958 (top) and a mid-type WN 5−6 star spectrum in the Milky Way (bottom). The figure shows the detection of the N III 4634 and the He II 4686 features, revealing the presence of WR stars in the galaxy.

shows the wavelength range 4450–4750 Å for the spectrum of the galaxy and a mid-type WN 5−6 star spectrum in the Milky Way (Paul Crowther, private communication). The aim of this figure is to compare the morphology of the two spectra in the relevant wavelength range. The figure shows the detection of the N III 4634 and the He II 4686 features in our spectrum, consistent with the presence of WR stars. The detection of such features indicates ongoing star formation activity in the case of IRAS 15130−1958. Among all the galaxies in our sample, this is the only case with a clear detection of WR features. Assuming that the VYSP component is associated with the WR features, the detection of these features provides a further constraint on the VYSP ages, i.e. the VYSP ages must be $\lesssim 10$ Myr. This is consistent with the lower end of the range of VYSP ages obtained from modelling the continuum.

IRAS 15206−3342. Bright knots are observed in the innermost region of this single nucleus system, and also spread over even larger scales, spanning a wide range of ages (from a few Myr up to 2 Gyr; Surace et al. 1998). This object is spectroscopically classified as an H II-like galaxy in the optical (Kim et al. 1998; Veilleux et al. 1999a). Moreover, no evidence for the presence of a buried AGN/quasar is found at IR and radio wavelengths (Veilleux et al. 1997; Nagar et al. 2003; Imanishi et al. 2007). The large nuclear Hα equivalent width and luminosity are also consistent with a starburst-dominated ionizing source (Arribas & Colina 2002). We find adequate fits for two groups of combinations of stellar populations. The VYSPs in the first group are younger than 3 Myr, while such component has an age of 10 Myr in the case of the second group. However, the large equivalent width of the Hα emission line [EW(Hα) = 315 Å], suggest VYSP ages of $t_{\mathrm{VYSP}} \lesssim 5$ Myr. This result favours the first group of adequate fits, including the younger VYSP component, which is also consistent with the upper limit of 20 Myr found by Farrah et al. (2005) on the basis of their UV/optical spectroscopic study of the stellar populations in the galaxy.

IRAS 15327+2340. Also known as Arp 220, this double nucleus system is the closest ULIRG in our sample ($z = 0.018$). The double nucleus structure is unresolved in our spectroscopic data. A biography and a detailed analysis of modelling results are presented for this object in RZ08. For completeness, the modelling results of

Comb I, Comb II and Comb III are shown in Tables 4, 6 and 8, respectively. The extraction apertures and the extracted spectra are also shown in Figs 2 and 3.

IRAS 15462−0450. Because of the powerful AGN emission, it was not possible to model the stellar populations in this compact ULIRG, which is classified as a Sy1 galaxy at optical wavelengths. The extraction aperture and the extracted 1D spectrum are shown in Figs 2 and 6.

IRAS 16156+0146. Three apertures were extracted for this double nucleus system, sampling the two nuclei and the region in between. The optical spectrum is that of a Sy2 galaxy, with the AGN activity associated with the north-western source. Moderately reddened, dominant VYSPs of age 9–10 Myr are found for that source (5 kpc-I). On the other hand, in the case of the south-eastern nucleus (5 kpc-II), the modelling results are consistent with wide ranges of age, reddening and percentage contribution for both the VYSPs and the IYSPs. It is notable that the minimum percentage contribution of the VYSPs found for the aperture 5 kpc-I (60 per cent) is significantly higher than in the case of Ap A and 5 kpc-II (20 and 15 per cent, respectively). These results suggest higher concentrations of VYSPs towards the north-west of the system, although we cannot rule out the idea of significant VYSPs at all locations.

IRAS 16474+3430. Three apertures were used for the analysis of the stellar populations in this double nucleus system, centred on the nuclei and the region in between. The modelling results found for the southern nucleus (5 kpc-I), the brightest at optical wavelengths, reveal the presence of moderately reddened VYSPs (t_{VYSP} = 7–8 Myr) that dominate the flux contribution at optical wavelengths. For the other two apertures, the VYSPs are divided into two groups: a younger group with ages in the range 6–8 Myr, and a second, older, group with ages in the range 50–90 Myr. However, IRAS 16474+3430 is classified as an H II galaxy, exhibiting H II-like region features at all locations covered by the slit. The values of the Hα equivalent widths (101, 49 and 69 Å for 5 kpc-I, 5 kpc-II and Ap A, respectively) are only attained for stellar populations of ~ 6.5 Myr. This is consistent with modelling results found for the southern nucleus (5 kpc-I), and the younger group of VYSPs in the cases of 5 kpc-II and Ap A.

IRAS 16487+5447. This galaxy is classified as a LINER galaxy (Kim & Sanders 1998) in the optical, and shows no evidence for a buried AGN at mid-IR wavelengths (Imanishi et al. 2007), consistent with a starburst as the power source (Lutz et al. 1999). Two slit positions were used during the observations of this double nucleus system. For the eastern nucleus, the modelling results are consistent with the combination of a dominant 'old' IYSP plus a VYSP with a wide range of ages and reddenings. It is notable that adequate fits are also obtained for this nucleus using Comb I, with a dominant 12.5-Gyr OSP. On the other hand, for the western source, we find VYSPs with relatively low reddening, which represent a large fraction of the optical emission from the galaxy. In addition, modelling the emission lines of the 5-kpc aperture for this source we find [O III]5007/Hβ and [N II]6583/Hα emission-line ratios consistent with an H II galaxy. The VYSP age obtained using the Hα equivalent width [EW(Hα) = 28 Å, $t_{\mathrm{VYSP}} \sim 7$ Myr] is consistent with the lower end of the range of ages found from the modelling. These results clearly demonstrate large differences between the stellar populations in the two nuclei. Finally, no clear evidence is found for the presence of age or reddening trends in the case of the western source.

IRAS 17028+5817. Again, two slit PAs were used during the observations of this system, sampling the two, widely separated (25 kpc) galaxies. We find that VYSPs make a large contribution, or even dominate, the flux at optical wavelengths in the two nuclei. However, in the case of the eastern galaxy, classified as an H ɪɪ galaxy, we find moderately reddened VYSPs that span a narrow range of ages. On the other hand, the modelling results are consistent with a wider range of ages and significantly higher reddening values for the VYSPs located in the western galaxy, which is classified as a LINER in the optical. The modelling results obtained for the eastern source are consistent with the age of ∼6 Myr estimated using the Hα equivalent width [EW(Hα) = 102 Å]. In addition, we extracted a third, extended aperture (labelled as Ap A in Fig. 2), sampling the region towards the south of that source. We do not find clear evidence suggesting the presence of large age or reddening variations.

IRAS 17044+6720. Classified as a LINER in the optical, this single nucleus system shows strong evidence for the presence of obscured AGN activity at mid-IR wavelengths (Imanishi et al. 2007). The modelling results found in the nuclear region of the galaxy are consistent with VYSPs of relatively low reddening, that make a large contribution to the flux at optical wavelengths. Comparing these results with those found for the extended apertures, we do not find clear evidence for the presence of significant age and/or reddening variations across the body of the galaxy. Note that Ap B (see Fig. 3) has line ratios typical of an H ɪɪ region ([N ɪɪ]6583/Hα = 0.24 and [O ɪɪɪ]5007/Hβ = 3.0). The estimated Hα equivalent width is EW(Hα) = 113 Å. Such high equivalent width is only attained for stellar populations younger than ∼6 Myr, which is consistent with the lower end of the age range obtained for Ap B from the continuum modelling.

IRAS 17179+5444. A single 5-kpc aperture was extracted for the analysis of the stellar populations in this single nucleus object. The optical spectrum of the nucleus is that of a Sy2 galaxy. The modelling results are consistent with a wide range of VYSPs ages, reddenings and percentage contributions.

IRAS 20414−1651. This galaxy is classified as a single nucleus system in the new *HST H*-band imaging survey carried out by Veilluex et al. (2006). Optically classified as an H ɪɪ galaxy (Kim & Sanders 1998), IRAS 20414−1651 shows no evidence for a buried AGN at near- and mid-IR wavelengths (Imanishi et al. 2007). Farrah et al. (2003) modelled optical and IR photometric data and found that almost the entire IR emission in this source is powered by the starburst. Our modelling results reveal the presence of an important contribution to the flux from relatively highly reddened VYSPs. The age of ∼6 Myr estimated using the Hα equivalent width [EW(Hα) = 43 Å] is consistent with the lower end of the age range obtained from the modelling.

IRAS 21208−0519. This double nucleus system is classified as an H ɪɪ galaxy in the optical. However, the northern nucleus, the brightest at optical and near-IR wavelengths, is the only region of the galaxy clearly showing H ɪɪ-like features in our spectra. The modelling results found for that nucleus (5 kpc-I) are consistent the presence of moderately reddened, dominant VYSPs. The Hα equivalent width found for that region of the galaxy [EW(Hα) = 45 Å] indicates VYSPs of age ∼6.6 Myr. This is consistent with the lower range of ages found from the modelling for this component. However, the modelling results found for southern nucleus (5 kpc-II), reveal the presence of a dominant 12.5-Gyr OSP plus an 'old' VYSP (90–100 Myr) with low reddening, that makes a small contribution to the flux in the optical. Intriguingly, an important contribution from
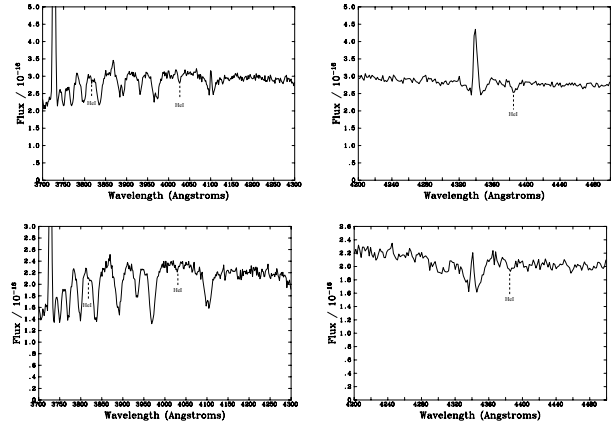

Figure A5. Extracted spectra from Ap B (upper panel) and Ap C (lower panel) for IRAS 22491−1808. The figure shows the detection of the He ɪ absorption lines at 3820, 4026 and 4388 Å. These lines are not observed in stellar populations older than 100 Myr.

a VYSP component is again required in order to model the extracted spectrum from Ap B, centred in the bright blob to the south of the galaxy (see Kim et al. 2002, their fig. 1). Finally, the modelling results for Ap A, sampling the region between the nuclei, are consistent with a mix of stellar populations from the two nuclei.

IRAS 21219−1757. This object is classified as a Sy1 galaxy at optical wavelengths. Therefore, due to the powerful AGN emission, it was not possible to model the stellar populations of this compact ULIRG. The extraction aperture and the extracted 1D spectrum are shown in Figs 2 and 3.

IRAS 22491−1808. Several knots and condensations located in both the tidal features and the nuclear region are visible in the high-resolution *BIHK'*-band images presented in Surace et al. (2000). The estimated ages cover a wide range from 5–7 Myr up to a few 100 Myr. With the optical spectrum of an H ɪɪ galaxy (Veilleux et al. 1995), IRAS 22491−1808 shows no signs of obscured nuclear activity at IR wavelengths (Genzel et al. 1998; Veilleux et al. 1999b; Imanishi et al. 2007) and it is therefore classified as a starburst-powered ULIRG (Lutz et al. 1999; Armus et al. 2007). Because of the small nuclear separation, and the fact that the slit is not perfectly aligned with the double nucleus structure, the 5-kpc aperture includes emission from both nuclei. Therefore, we decided to use another two apertures to sample the eastern (Ap B) and western (Ap C) nuclei individually.

The modelling results found for both nuclei are consistent with the presence of moderately reddened VYSPs that make an important contribution, or even dominate, the flux at optical wavelengths. Unsurprisingly, the modelling results for the 5-kpc aperture are consistent with the mix of stellar population in the two nuclei. The VYSP age determined from the Hα equivalent widths (64 and 46 Å for Ap B and C, respectively, corresponding to VYSPs of age ∼6.5 Myr) is consistent with the results obtained from the modelling. Furthermore, the extracted spectra for Ap B and Ap C (and also 5 kpc) show the clear presence of He ɪ absorption features at various wavelengths, which are indicated in Fig. A5. These lines are not observed in stellar populations older than 100 Myr and, therefore, provide further evidence for the presence of significant VYSPs in the two nuclei of the galaxy. Finally, Ap A was extracted to sample the tidal tail towards the north-west of the galaxy. Overall we do not find clear evidence for the presence

of significant age/reddening gradients across the body of the galaxy.

IRAS 23060+0505. This single nucleus system is classified as a Sy2 in the optical, and shows clear signatures of AGN activity at mid-IR wavelengths (Genzel et al. 1998; Lutz et al. 1999). For the nuclear region adequate fits are only obtained using Comb II, including a 10-Myr VYSP, a 'red' power-law component (index $\alpha = 6.1$) and a 12.5-Gyr OSP making contributions to the optical light of 72, 6 and 22 per cent, respectively. It is worth remembering that these are percentage contributions in the normalizing bin, which in the case of IRAS 23060+0505 is located at a wavelength range of 4450–4550 Å. The contribution of the power-law component becomes more important with increasing wavelength, and is as high as 43 per cent at 6800 Å. This is consistent with the results of Veilleux et al. (1997) who found a strong broad Paα line at near-IR wavelength, providing evidence for a significant contribution from a highly obscured AGN. For the other two apertures, Ap A and Ap B, adequate fits are obtained using all combinations (i.e. the YSP properties are relatively unconstrained).

IRAS 23233+2817. Kim et al. (2002) described this object as 'the only object in the 1-Jy sample with no obvious signs of interaction'. Our Ap A samples a region to the south of the nucleus, including the bright knot detected in the Kim et al. (2002) *K*-band image. These authors described the latter as a bright H II regions on the basis of its luminosity and colour. However, we identified this knot as an M star in the galaxy based in our spectroscopic data (see Fig. 3). In the case of the 5-kpc aperture, adequate fits were obtained using Comb I and Comb II, but not Comb III. Since the galaxy is classified as a Sy2, we concentrate on the results of Comb II. We find YSPs in combination with a 12.5-Gyr OSP, and power-law that makes a significant contribution to the flux at optical wavelengths. These results suggest that the AGN component is important in the case of IRAS 23233+2817.

IRAS 23234+0946. This double nucleus system is classified as a LINER on the basis of its optical spectrum. The western source is the brightest at optical wavelengths, and shows no sign of AGN activity in the mid-IR (Imanishi et al. 2007). The modelling results found for this nucleus (5 kpc-I) are consistent with the presence of VYSPs that dominate the flux in the optical. Comparing these results with those of the other two apertures, it is notable that the percentage contribution of the VYSP component in the western nucleus (60–82 per cent) is significantly higher than in the eastern nucleus and the extended structure to the east of the galaxy (17–37 per cent). Intriguingly, while high reddening values are found for the VYSP component $[E(B - V) = 0.5–1.5]$ to the east of the galaxy (5 kpc-II and Ap A), lower reddening values $[E(B - V) = 0.4–0.6]$ are found for the western source.

IRAS 23327+2913. Initially, two 5-kpc apertures were extracted sampling the two nuclei of this double nucleus system. In order to look for possible variations of the stellar populations within the galaxy when sampling larger regions, two additional, wider apertures were extracted, also centred on each nucleus. The extracted spectra for these apertures are identical to those of the 5-kpc apertures and therefore are not shown in Fig. 3. In the case of the southern source (5 kpc-I) an OSP is always required in order to model the extracted spectrum. The modelling results of Comb I are consistent with a mix of a 12.5-Gyr OSP plus a moderately reddened VYSP of 9 Myr that dominates the flux at optical wavelengths. On the other hand, this object is classified as a LINER at optical wavelengths and shows no evidence for a buried AGN (Imanishi et al. 2007). Therefore, it is likely that the power-law component used in Comb II accounts for a VYSP in this case, and it is possible that we are detecting the contribution of three different stellar components to the optical light: a 12.5-Gyr OSP plus important contribution from a highly reddened VYSP younger than ∼5 Myr (represented by a power-law with power-law index $\alpha = 1.54$) and a VYSP of age 10 Myr and lower reddening. In the case of the northern galaxy (5 kpc-II), it is possible to model the extracted spectrum using a single OSP of age 12.5 Gyr, with no need for any additional stellar component. Again, an OSP is always required to model the data. This demonstrates large differences between the stellar populations in the two nuclei.

IRAS 23389+0300. The northern source of this double nucleus system is the brightest galaxy in the radio, known to have a milliarc-second radio core and extended radio emission (Nagar et al. 2003). Two 5-kpc apertures were extracted for this Sy2 galaxy, centred on the two nuclei. In order to perform a more detailed analysis of the stellar populations, an additional set of four smaller apertures was extracted sampling various regions of the galaxy. The extracted spectra from Ap B and Ap D are identical to those of 5 kpc-I and 5 kpc-II, and hence, they are not shown in Fig. 3. The modelling results suggest the presence of younger VYSPs towards the north of the system, although we cannot rule out the idea of VYSPs of similar age at all locations sampled by the various apertures. In terms of reddening, we find no clear evidence for the presence of significant variations across the body of the galaxy.

This paper has been typeset from a TEX/LATEX file prepared by the author.